NEA/NSC/DOC(95)03/I
Volume I

PU-MET-INTER-002

ZPR-6 ASSEMBLY 10:
A CYLINDRICAL PLUTONIUM/CARBON/STAINLESS STEEL ASSEMBLY WITH STAINLESS STEEL AND IRON REFLECTORS

Evaluators

Richard M. Lell, Micheal A. Smith,
Robert W. Schaefer, and Richard D. McKnight
Argonne National Laboratory

Internal Reviewers
Richard M. Lell and Micheal A. Smith

Independent Reviewers

Margaret A. Marshall
Idaho National Laboratory

Reuven L. Perel and Jehudah J. Wagschal
Racah institute of Physics
The Hebrew University of Jerusalem

ACKNOWLEGEMENT

This work was supported by the U.S. Department of Energy, Office of Nuclear Energy, Task 82232, under contract no. DE-AC02-06CH11357.

PU-MET-INTER-002

ZPR-6 ASSEMBLY 10: A CYLINDRICAL PU/C/SST ASSEMBLY WITH STAINLESS STEEL AND IRON REFLECTORS

IDENTIFICATION NUMBER: PU-MET-INTER-002 SPECTRA

KEY WORDS: acceptable, assembly, critical experiment, cylinder, fast, graphite, heterogeneous, intermediate spectra, metal, plates, plutonium, reflected, ZPR

1.0 DETAILED DESCRIPTION

1.1 Overview of Experiment

The Pu/C/SST Benchmark Assembly was part of the Diagnostic Cores Program planned for the Argonne National Laboratory (ANL) ZPR-6 and ZPR-9 critical facilities.[a] The objective of the Diagnostic Cores Program was to resolve longstanding discrepancies between calculated and measured values for small-sample central worths, β_{eff}, and the ^{238}U capture-to- ^{239}Pu fission reaction rate ratio (c^{28}/f^{49}). The Diagnostic Cores Program consisted of two phases. Phase I was a definitive investigation of one cause of the central worth discrepancy, namely, the effects of heterogeneities in the vicinity of the samples which are not treated by the calculations. Phase II was planned to find the dependence on composition and spectrum of these three discrepancies. The Pu/C/SST Benchmark Assembly was the third and last assembly in the Phase II Diagnostic Cores Program.

Because the Phase II Program encompassed a wide range of spectra and emphasized strongly the reactor materials of greatest importance to the discrepant parameters, these assemblies provide excellent systems for criticality-safety validation. The first assembly of the Phase II Diagnostic Cores Program was the U/Fe Benchmark Assembly (ZPR-9/34), which has been included in this Handbook as benchmark HEU-MET-INTER-001. The second assembly of the Phase II Diagnostic Cores Program was the U9 Benchmark Assembly (ZPR-9/36, ZPR-6/9), which has been included in this Handbook as benchmark IEU-MET-FAST-010. The third assembly of the Phase II Diagnostic Cores Program was the Pu/C/SST Benchmark Assembly (ZPR-6/10). This assembly had a heterogeneous cylindrical core constructed of plutonium metal fuel (critical mass 178.5 kg ^{239}Pu + ^{241}Pu) with carbon/stainless steel diluents; an axial reflector of stainless steel; an inner radial reflector of stainless steel; and an outer radial reflector of iron. This core was the only assembly built on either ZPR-6 or ZPR-9 to be fueled entirely with Pu/Al metal fuel (1.1 w/o Al), which is enriched to 95.3 a/o ^{239}Pu/Pu.

Experiments were performed in the Pu/C/SST Benchmark Assembly built in the ZPR-6 facility between August 1981 and July 1982. The particular configuration of ZPR-6/10 selected as being most suitable to form a criticality-safety benchmark has the designation Loading 24.

The term “benchmark” in a ZPR program connotes a particularly simple loading aimed at gaining basic reactor physics insight, as opposed to studying a reactor design. In fact, the Pu/C/SST Benchmark Assembly had a very uniform core assembled entirely from a single core unit cell loaded into stainless steel drawers

[a] ZPR is an acronym for Zero Power Reactor, referring to the four very similar fast-reactor critical experiment facilities at Argonne, two of which were the ZPR-6 and ZPR-9 facilities. A brief and simple description of these facilities is included in the American Nuclear Society monograph by W. G. Davey and W. C. Redman, *Techniques in Fast Reactor Critical Experiments*, Gordon and Breach, Science Publishers, Inc., New York (1970).

that were then loaded into the ZPR-6 matrix. The core unit cell had a simple loading whose neutronic characteristics were dominated by ^{239}Pu. Many of the experiments involved measuring, in both traditional and novel ways, the reactivity associated with introducing a small sample of fissile material near the center of the assembly. Some of these experiments required unusually careful measurements of criticality.

This assembly provides a useful benchmark for testing criticality calculations. As just noted, ^{239}Pu dominated the neutronic behavior in the core region. About 99% of the fissions and ~76% of the absorptions in the core were in ^{239}Pu – with most of the remaining absorptions in the steel. The inclusion of graphite in the core unit cell moderated the spectrum more than the traditional ZPR fast reactor cores. Although the bulk of the neutron spectrum is in the 10-keV to 2-MeV energy range with a broad peak in the 100-500 keV range, there is significant flux below 10 keV. About 65% of the fissions occur at energies between 0.625 ev and 100 keV, so the spectrum is in the intermediate range. As would be expected, the neutron balance for this assembly is dominated by ^{239}Pu (see Appendix C).

A very accurate transformation to a simplified model is needed to make any of the ZPR assemblies a practical criticality-safety benchmark. There is simply too much geometric detail in an exact model of a ZPR assembly – even a clean benchmark such as ZPR-6/10 Loading 24. The transformation must reduce the detail to a practical level without masking any of the important features of the criticality experiment. And it must do this without increasing the total uncertainty far beyond that of the original experiment. Such a transformation is described in Section 3. It was made using a pair of continuous-energy Monte Carlo calculations. First, Loading 24 was modeled in full detail – every plate, drawer, matrix tube, and air gap was modeled explicitly. Then the regionwise compositions and volumes from this model were used as a homogeneous, two-dimensional (RZ) model. This simple model is the criticality-safety benchmark model. The difference in k_{eff} values between the two models was used to adjust the measured excess reactivity of Loading 24, yielding a result for the benchmark model. The net difference in k_{eff} and each of the effects that contribute to it are small (<2%). Uncertainties associated with this simplification, which go beyond Monte Carlo statistical uncertainties, have been estimated and determined to be acceptably small (~0.2%).

1.2 Description of Experimental Configuration

The result for the excess reactivity measurement for Loading 24, which was recorded in the experiment logbook on 30 September 1981,[a] was 75.087 ± 0.615 inhours (Ih), which is quite small[b] (see Section 2.1). This excess is after correction to a temperature of 25°C and adjustment to a reference table closure. Later in the experimental program, the isothermal temperature coefficient (determined to be a function of whether the cooling fans were on or off and of the reactor power level) was measured to be –4.82 Ih/°C.[c] Note that an inhour is the amount of positive reactivity that produces a stable period of one hour. The inhour is rarely (if ever) used today, but it was a common reactivity unit for experimental measurements when ZPR-6 operated.

A lot of details must be presented to describe precisely the as-built assembly. Also, it is useful to define some jargon (to be shown in italics) to facilitate the presentation. For those unfamiliar with ZPR assemblies, the task of absorbing this may be tedious if not a bit overwhelming. In fact, the task of modeling the exact plate-by-plate loading would be unreasonable to do by hand. In practice, the information contained in this section was accumulated in an electronic database and processed into models using computer programs. Readers interested only in using the benchmark model need not be concerned with any of these details, since Section 3 contains a complete specification of the criticality-safety benchmark model.

[a] Applied Physics Division Experiment Logbook, APD-32, Argonne National Laboratory, 1981.
[b] J. R. Lamarsh, *Introduction to Nuclear Reactor Theory*, p. 439, Addison-Wesley, Reading, MA (1966).
[c] Private communication, R. B. Pond and R. A. Scharping, Argonne National Laboratory, February 1, 1982.

1.2.1 The ZPR-6 Facility - The ZPR-6 fast critical facility was a horizontal split-table type machine consisting of a large, cast-iron bed supporting two tables, one stationary and the other movable.[a,b] A pictorial view of the ZPR-6 facility is shown in Figures 1-1 and 1-2. Each table was 12 feet (3.7 m)[c] wide and 8 feet (2.4 m) long. During loading operations, the tables were separated by 5 feet (1.5 m). In operation, the movable table was driven against the stationary table with a nut and lead screw mechanism. Stainless steel square tubes, 0.040 inches (1 mm) thick, 2.175 inches (55 mm) on a side (outside dimension) and 4 feet (1.2 m) long, were welded in 5-tube by 5-tube bundles and stacked horizontally on both tables to form a 65-row and 65-column square "honeycomb" matrix.[d] The picture of the facility in Figure 1-1 shows the ZPR-6 matrix before it was expanded from 45 rows and 45 columns. The expansion of the matrix was completed just prior to the loading of ZPR-6 Assembly 9. A *matrix position* is specified by three parameters: matrix half (S or M), row number (starting from the top) and column number (starting from the left looking from the movable half towards the stationary half). For example, the central position in the movable half is M-33/33. The matrix tubes were supported on the sides by massive cast-iron structures known as the knees. A mild-steel back plate, about 28.7 inches (72.8 cm) behind the matrix tubes on each table, supported the control rod drives. The drives were mounted on the outboard side of the plate and were connected to control rods by steel shafts. Between the matrix tubes and back plate on each table was a plenum region, which provided a flow path for cooling air into and out of the matrix. The matrix machine was near the center of a large cell (room), approximately 40 feet by 30 feet and 30 feet tall (9 x 9 x 12 m).

The desired average composition was achieved by loading the matrix with drawers containing rectangular plates (or, in some assemblies, with cylindrical rods) of different materials such as depleted, enriched, or natural uranium; stainless steel; sodium, etc. A specific plate-loading pattern in a drawer is called a *drawer master*. The plates were bare material or had a cladding or, in the case of uranium, had a protective coating. Figure 1-3 is an illustration of the plates inside the drawers and matrix forming a unit cell for a particular region in a particular loading (not ZPR-6/10). The specification of which drawer master was in each matrix position is known as a *matrix loading map*.

It was usually the case that a given matrix position had two drawers, a *front drawer* and a *back drawer*. Correspondingly, there would be two matrix loading maps for each half, a front map and a back map. However, except for the neutron source locations, no back drawers were used in ZPR-6/10. The entire core and radial reflector regions used 36.252-inch-long (920.8-mm) stainless steel drawers. The core loading was in the first 15-inch portion of these drawers. The axial reflector region filled the following 21-inch portion. The radial reflector regions were built with the same type of drawers, which were fully loaded with 36 inches of either stainless steel or iron blocks.

[a] W. Y. Kato et al., "Final Safety Analysis Report on the Use of Plutonium in ZPR-6 and -9," Argonne National Laboratory Report, ANL-7442 (February 1970).
[b] Private communication, R. B. Pond, Argonne National Laboratory, November 15, 1979.
[c] Almost all of the references give dimensions in English units and some also give metric equivalents. We display the metric equivalent in parentheses when practical, as a courtesy to international readers.
[d] Imperfect alignment of the matrix bundles produces a gap at the interface when the tables are driven to the "closed" position.

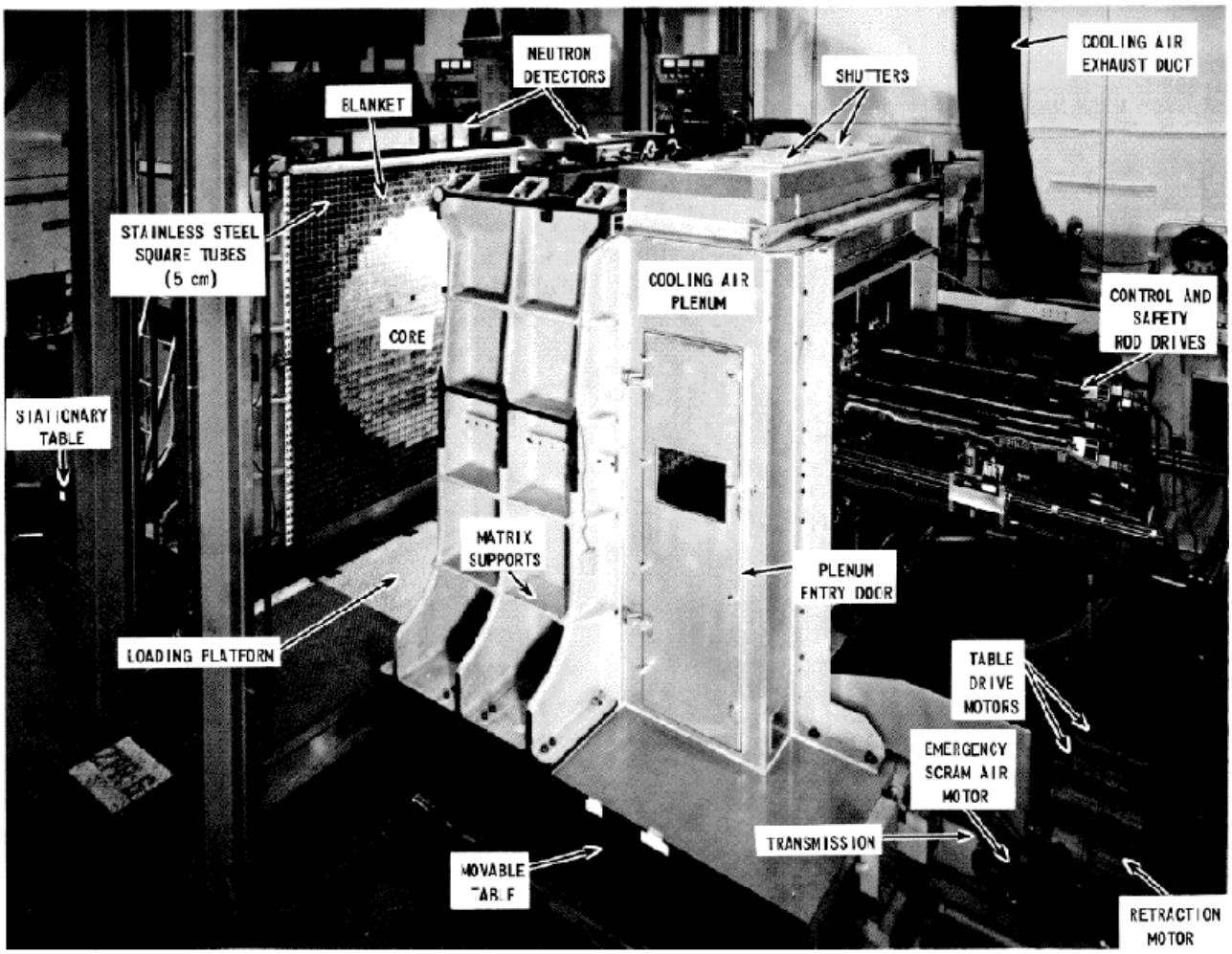

Figure 1-1. View of the ZPR-6 Facility
(photograph prior to enlargement of matrix).

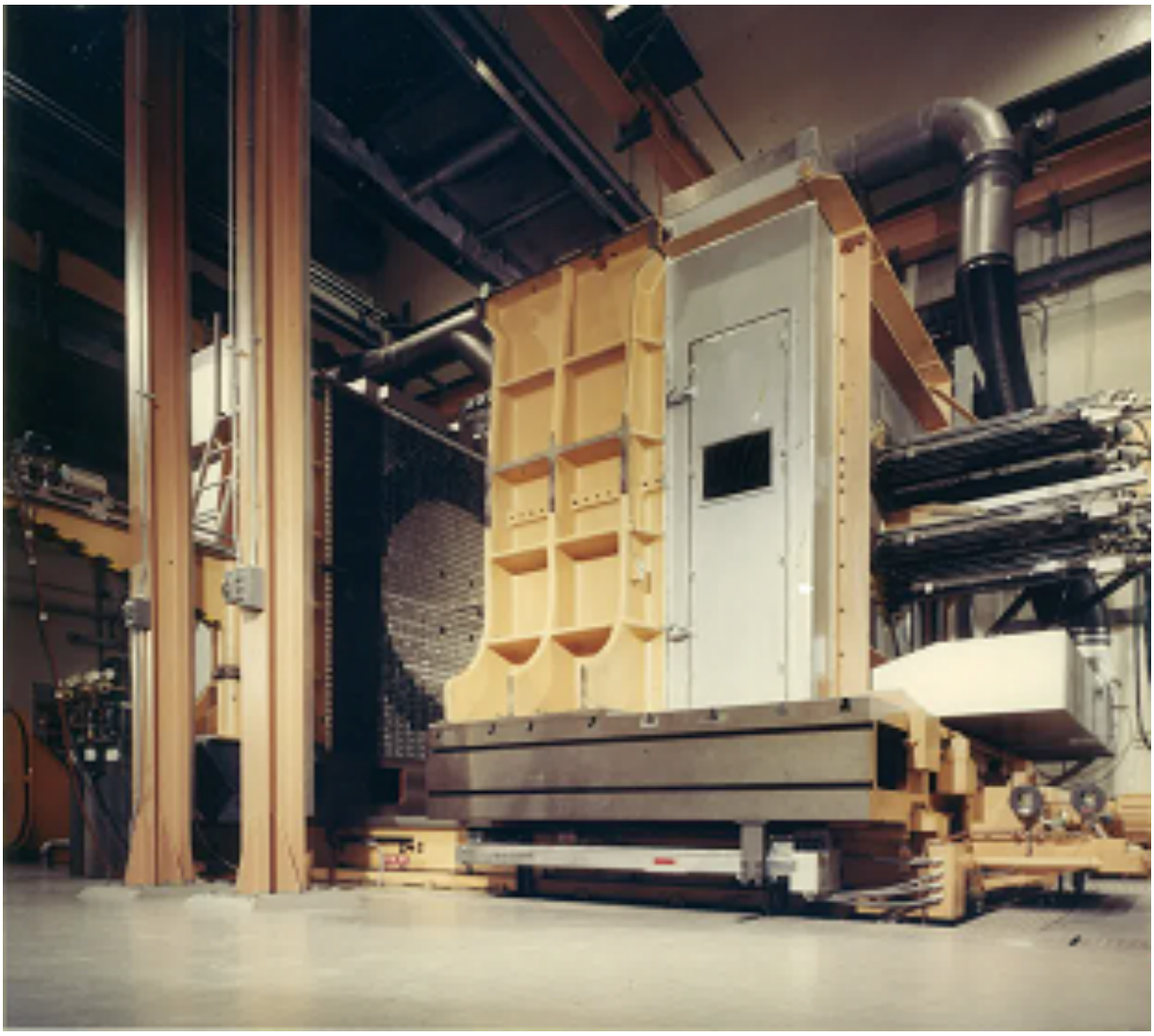

Figure 1-2. ZPR-6 Split Table Critical Assembly.

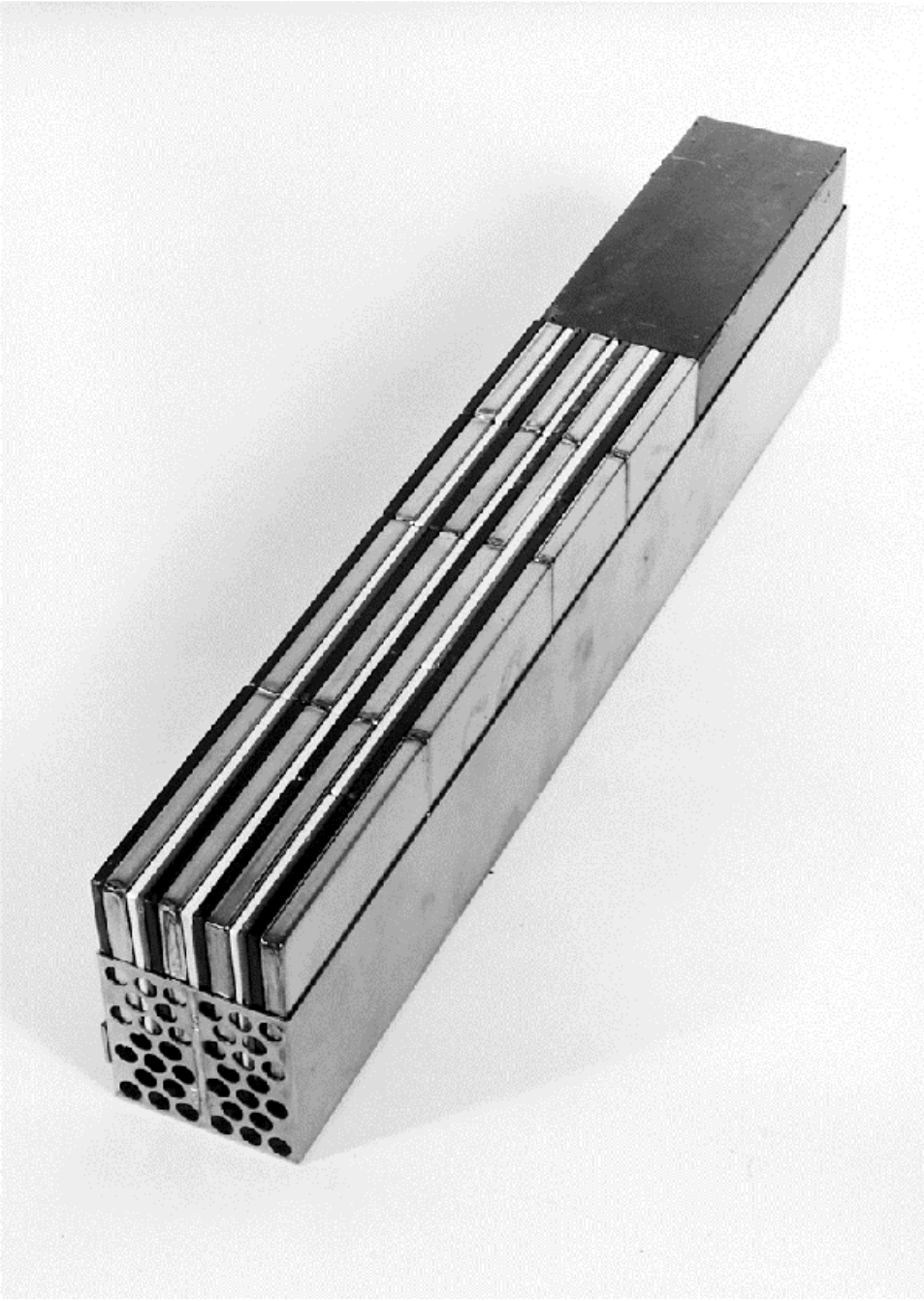

Figure 1-3. Typical ZPR Drawer.[a]

[a] The plates are elevated above the bottom of the drawer in this photograph. This drawer was not used in ZPR-6/10.

There were usually many plate sizes available for a given material and a limited number of plates of any one size. Consequently, there were often several drawer masters that had essentially the same composition, differing only in the plate sizes used. The number of similar drawer masters was magnified by the fact that drawers for the stationary and movable halves had different (opposite, mirror image) drawer masters.

The ZPR drawers themselves typically were made of 0.03-inch-thick (0.8-mm) stainless steel, and their front, back, and side walls were 2 inches (51 mm) tall. Control drawers were also made of stainless steel, but could be of a slightly different construction (e.g., thicker walls, reduced width, etc.).

Typically, two types of control rods were used in a ZPR assembly. One type was the *dual-purpose* (DP) control rod, so-called because it was a drawer that contained a core unit cell but could be driven in and out along a matrix tube to adjust reactivity. There were no control rods of this type in ZPR-6 Assembly 10. The other type of control rod was the *poison safety rod* (PSR), which contained a blade of boron powder or B_4C clad with stainless steel, 3/8 inch (9.5 mm) wide by 1.94 inches (49 mm) tall, that traveled in a thin-walled stainless steel guide tube. The rest of the matrix tube containing a PSR was filled by a stationary, narrow drawer with a plate loading as similar as possible to the unit cell of the region. The blade could be attached either to a scram-type drive or to a drive used for fine reactivity control. For the Pu/C/SST Benchmark Assembly, only PSR control rods were used. There were eight PSR rods per half in ZPR-6/10. In each half, four of these PSR rods were located in the outermost row of the core; the remaining four were located in the steel radial reflector in positions adjacent to the core. For Loading 24 the blades were in their withdrawn positions, approximately 15 inches past the core/axial reflector interface.

Temperature monitoring of the core was done using *thermocouple drawers*. In this type of drawer master, small thermocouples were attached to fuel plates in several places along a fuel column. The adjacent plate column had to be less than full height to allow room for the thermocouples and wires. There were three of these special drawers per half in ZPR-6/10.

A neutron source had to be present in each matrix half during the startup of any ZPR assembly not containing an inherent source in the core (e.g., ^{240}Pu). Even though its Pu/Al fuel contained a spontaneous fission source, the Pu/C/SST Benchmark Assembly had source tubes that ran axially within one front-back drawer combination per half. Sources were driven close to the core through these two tubes at startup and withdrawn once criticality was achieved.

The full details of a ZPR loading are not usually contained in published reports because of their complexity. Instead, it was usual to give details of a representative drawer master for each region, the matrix loading map in terms of the representative drawer masters, and the average composition for each material region. However, the detailed description was archived in loading records, both electronic and paper.

1.2.2 The Matrix and Drawer Loading Data – A general matrix loading diagram for ZPR-6/10 Loading 24 is shown in Figure 1-4. This figure provides the general region boundaries, as well as the locations of the poison safety rods and thermocouples.

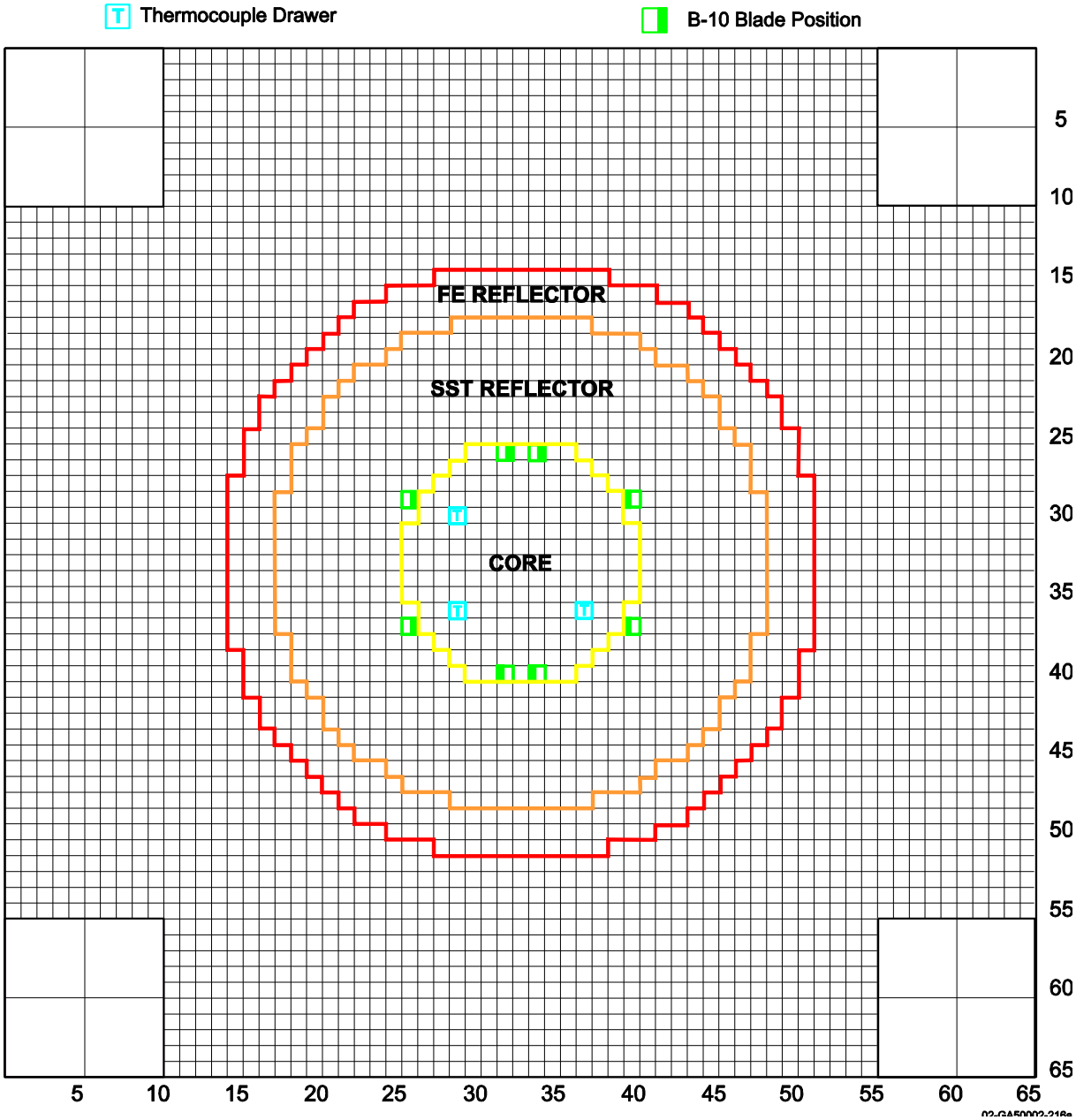

Figure 1-4. ZPR-6 Assembly 10 (Loading No. 24) Reference Configuration Matrix Loading.

An idea of what the loading was like at the plate level is given in Figure 1-5. This figure is a slice through a matrix position in the core region, showing the matrix tube, drawer and plates, forming a unit cell. The small gap between the top of the plates and the bottom of the upper wall of the matrix tube served as a flow path for cooling air. The standard plate loading in the core region consisted of 1 column (plates) of plutonium/aluminum metal fuel centered in the drawer between alternating symmetric columns of stainless steel and carbon. The Pu/Al plates were each 1/8-inch-thick; the remainder of the 2-inch width of the unit cell contained six 1/8-inch-thick carbon plate columns, four ¼-inch-thick stainless steel plate columns and two 1/16-inch-thick stainless steel plate columns.

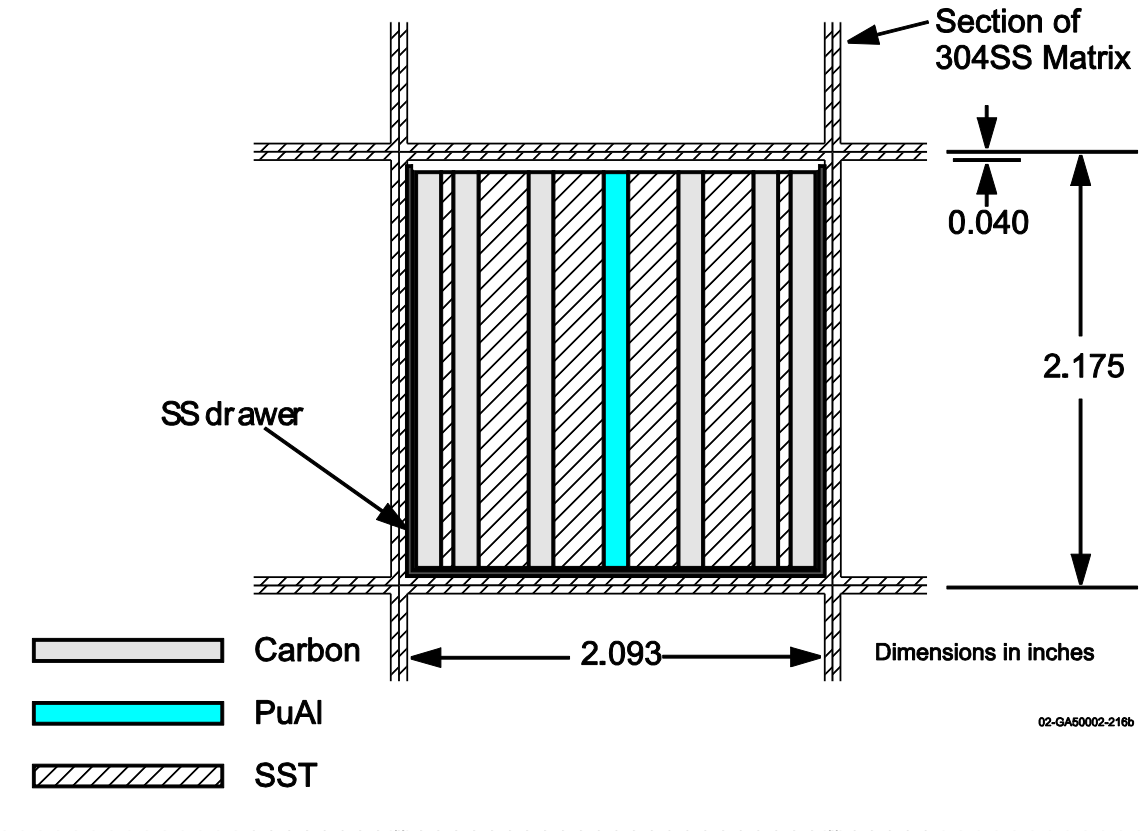

Figure 1-5. Cross Section of Core Unit-Cell Showing Matrix and Plate-loaded Drawer of ZPR-6 Assembly 10.

Details of the specific drawer loaded into each matrix location of both the movable and stationary halves of the assembly are given in Figures 1-6 and 1-7. A unique number is used there to represent each drawer master. A broad look at this figure reveals large portions dominated by a single number, i.e., by one drawer master. Several tables are used to define completely the drawer masters represented by each of the numbers in Figures 1-6 and 1-7. Table 1.1 gives the identification number used in Figures 1-6 and 1-7, the corresponding ZPR drawer-master number,[a] the length and type of drawer, and the number of occurrences of this drawer master in Loading 24. Note that when Table 1.1 associates a pair of drawer master numbers for a single identification symbol (such as 1001-FS-2 and 1001-FM-2 with the number "2"), the plate loadings for these drawers are identical due to their symmetry. Tables 1.2 and 1.3 provide the remainder of the geometric detail about each drawer master. Table 1.2 covers the entire group of drawer masters loaded in the core region; Table 1.3 covers all of the drawer masters loaded in the radial reflector regions. In each table the drawer masters are identified both in terms of the number in Figures 1-6 and 1-7 and by the drawer master number. The interpretation of the information will be illustrated by explaining the first drawer master in Table 1.2 with the aid of the corresponding drawer master diagram.

[a] In the nomenclature for drawer master numbers, FM indicates a front drawer in the movable half, FS indicates a front drawer in the stationary half, BM indicates a back drawer in the movable half, and BS indicates a back drawer in the stationary half. As noted previously, except for the neutron source locations, no back drawers were used in ZPR-6/10.

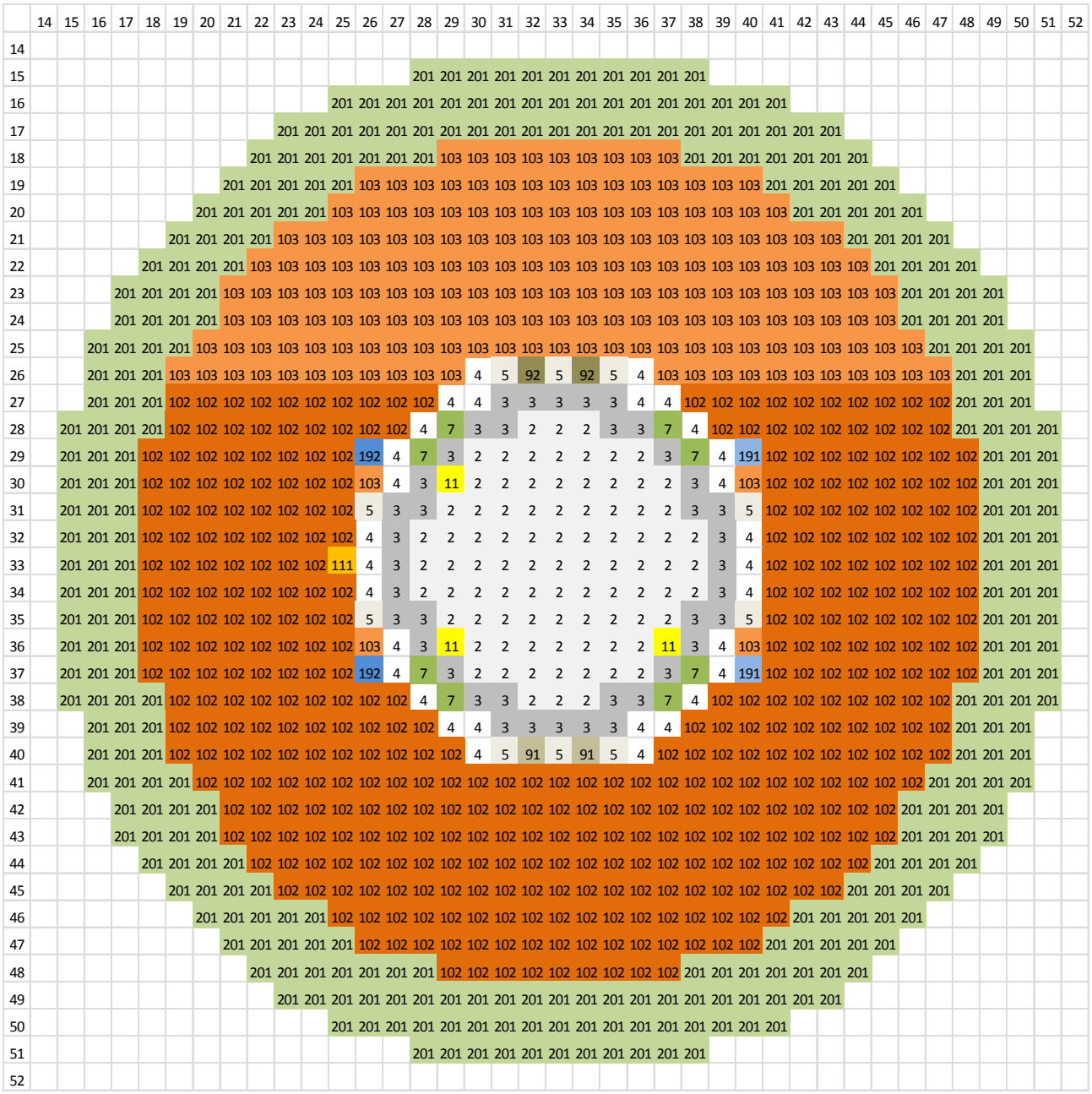

Figure 1-6. ZPR-6/10 Loading 24 – Half 1/Stationary Half.

	52	51	50	49	48	47	46	45	44	43	42	41	40	39	38	37	36	35	34	33	32	31	30	29	28	27	26	25	24	23	22	21	20	19	18	17	16	15	14
14																																								
15															201	201	201	201	201	201	201	201	201	201	201														
16												201	201	201	201	201	201	201	201	201	201	201	201	201	201	201	201	201	201										
17										201	201	201	201	201	201	201	201	201	201	201	201	201	201	201	201	201	201	201	201	201								
18									201	201	201	201	201	201	201	103	103	103	103	103	103	103	103	103	201	201	201	201	201	201	201								
19								201	201	201	201	201	103	103	103	103	103	103	103	103	103	103	103	103	103	103	103	201	201	201	201	201							
20							201	201	201	201	201	103	103	103	103	103	103	103	103	103	103	103	103	103	103	103	103	103	201	201	201	201	201						
21						201	201	201	201	103	103	103	103	103	103	103	103	104	104	104	104	104	103	103	103	103	103	103	103	103	201	201	201	201					
22					201	201	201	201	103	103	103	103	101	101	104	104	104	104	104	104	104	104	104	104	104	104	104	103	103	103	103	201	201	201	201				
23				202	201	201	201	101	101	101	101	101	101	101	104	104	104	104	104	104	104	104	104	104	104	104	104	104	104	104	104	201	201	201	202				
24				202	201	201	201	101	101	101	101	101	101	101	104	104	104	104	104	104	104	104	104	104	104	104	104	104	104	104	104	201	201	201	202				
25			202	202	201	201	101	101	101	101	101	101	101	101	104	104	104	104	104	104	104	104	104	104	104	104	104	104	104	104	104	201	201	202	202				
26			202	202	201	101	101	101	101	101	101	101	101	101	101	101	4	5	92	5	92	5	4	101	101	101	101	101	101	101	101	101	101	201	202	202			
27			202	202	201	101	101	101	101	101	101	101	101	101	101	4	4	3	3	3	3	3	4	4	101	101	101	101	101	101	101	101	101	201	202	202			
28		202	202	202	201	101	101	101	101	101	101	101	101	101	4	7	3	3	2	2	2	3	3	7	4	101	101	101	101	101	101	101	101	201	202	202	202		
29		202	202	202	101	101	101	101	101	101	101	101	191	4	7	3	2	2	2	2	2	2	3	7	4	192	101	101	101	101	101	101	101	101	202	202	202		
30		202	202	202	101	101	101	101	101	101	101	101	103	4	3	2	2	2	2	2	2	2	11	3	4	103	101	101	101	101	101	101	101	101	202	202	202		
31		202	202	202	101	101	101	101	101	101	101	101	5	3	3	2	2	2	2	2	2	2	2	3	3	5	101	101	101	101	101	101	101	101	202	202	202		
32		202	202	202	101	101	101	101	101	101	101	101	4	3	2	2	2	2	2	2	2	2	2	2	3	4	101	101	101	101	101	101	101	101	202	202	202		
33		202	202	202	101	101	101	101	101	101	101	101	4	3	2	2	2	2	2	2	2	2	2	2	3	4	111	101	101	101	101	101	101	101	202	202	202		
34		202	202	202	101	101	101	101	101	101	101	101	4	3	2	2	2	2	2	2	2	2	2	2	3	4	101	101	101	101	101	101	101	101	202	202	202		
35		202	202	202	101	101	101	101	101	101	101	101	5	3	3	2	2	2	2	2	2	2	2	3	3	5	101	101	101	101	101	101	101	101	202	202	202		
36		202	202	202	101	101	101	101	101	101	101	101	103	4	3	11	2	2	2	2	2	2	11	3	4	103	101	101	101	101	101	101	101	101	202	202	202		
37		202	202	202	101	101	101	101	101	101	101	101	191	4	7	3	2	2	2	2	2	2	3	7	4	192	101	101	101	101	101	101	101	101	202	202	202		
38		202	202	202	202	101	101	101	101	101	101	101	101	101	4	7	3	3	2	2	2	3	3	7	4	101	101	101	101	101	101	101	101	101	202	202	202	202	
39			202	202	202	101	101	101	101	101	101	101	101	101	101	4	4	3	3	3	3	3	4	4	101	101	101	101	101	101	101	101	101	101	202	202	202		
40			202	202	202	101	101	101	101	101	101	101	101	101	101	101	4	5	91	5	91	5	4	101	101	101	101	101	101	101	101	101	101	101	202	202	202		
41			202	202	202	201	101	101	101	101	101	101	101	101	101	101	101	101	101	101	101	101	101	101	101	101	101	101	101	101	101	101	101	201	202	202	202		
42				202	202	201	201	101	101	101	101	101	101	101	101	101	101	101	101	101	101	101	101	101	101	101	101	101	101	101	101	101	201	201	202	202			
43				202	202	201	201	101	101	101	101	101	101	101	101	101	101	101	101	101	101	101	101	101	101	101	101	101	101	101	101	201	201	201	202				
44					202	201	201	201	101	101	101	101	101	101	101	101	101	101	101	101	101	101	101	101	101	101	101	101	101	101	201	201	201	202					
45						201	201	201	201	101	101	101	101	101	101	101	101	101	101	101	101	101	101	101	101	101	101	101	101	201	201	201	201						
46							201	201	201	201	201	101	101	101	101	101	101	101	101	101	101	101	101	101	101	101	101	201	201	201	201	201							
47								201	201	201	201	201	101	101	101	101	101	101	101	101	101	101	101	101	101	101	201	201	201	201	201								
48									201	201	201	201	201	201	201	101	101	101	101	101	101	101	101	101	201	201	201	201	201	201	201								
49										201	201	201	201	201	201	201	201	201	201	201	201	201	201	201	201	201	201	201	201										
50												201	201	201	201	201	201	201	201	201	201	201	201	201	201	201	201	201											
51															201	201	201	201	201	201	201	201	201	201	201														
52																																							

Figure 1-7. ZPR-6/10 Loading 24 – Half 2/Movable Half.

Table 1.1. Drawer Identification and Type Data.

Identification Number	Drawer Master Number	Role of Drawer	Length (inches)	Type of Drawer	Number in Loading 24
Core Drawer Masters					
2	1001-FS-2 1001-FM-2	Normal Core	36.252	SST	172
3	1001-FS-3 1001-FM-3	Normal Core	36.252	SST	80
4	1001-FS-4 1001-FM-4	Normal Core	36.252	SST	60
5	1001-FS-5 1001-FM-5	Normal Core	36.252	SST	20
7	1001-FS-7 1001-FM-7	Normal Core	36.252	SST	16
11	1001-FS-11	Thermocouple	36.252	SST	3
11	1001-FM-11	Thermocouple	36.252	SST	3
91	1001-FS-10L	Core PSR	36.252	SST	2
92	1001-FS-10R	Core PSR	36.252	SST	2
91	1001-FM-10L	Core PSR	36.252	SST	2
92	1001-FM-10R	Core PSR	36.252	SST	2
Radial Stainless Steel Reflector Drawer Masters					
101	1010-FS-1 1010-FM-1	Radial Reflector	36.252	SST	449
102	1010-FS-2 1010-FM-2	Radial Reflector	36.252	SST	403
103	1010-FS-3 1010-FM-3	Radial Reflector	36.252	SST	257
104	1010-FS-4 1010-FM-4	Radial Reflector	36.252	SST	73
191	1010-FS-10L	Reflector PSR	36.252	SST	2
192	1010-FS-10R	Reflector PSR	36.252	SST	2
191	1010-FM-10L	Reflector PSR	36.252	SST	2
192	1010-FM-10R	Reflector PSR	36.252	SST	2
111	1010-FS-11	Neutron Source	24.375	SST	1
111	1010-FM-11	Neutron Source	24.375	SST	1
P[(a)]	1030-BS-1	Neutron Source	23.252	SST	1
Q[(a)]	1030-BM-1	Neutron Source	23.252	SST	1
Radial Iron Reflector Drawer Masters					
201	1020-FS-1 1020-FM-1	Radial Reflector	36.252	SST	569
202	1020-FS-2 1020-FM-2	Radial Reflector	36.252	SST	111

(a) Drawer master 1030-BS-1 was the back drawer behind front drawer 1010-FS-11, and drawer master 1030-BM-1 was the back drawer behind front drawer 1010-FM-11. These were the only back drawers used in ZPR-6/10 Loading 24.

Table 1.2. Core Drawer Plate Loading Descriptions.

Plate ID (size in inches)	Starting X location	Starting Y location	Starting Z location	X #	Y #	Z #
Identification Number 2, Drawer Masters 1001-FS-2 and 1001-FM-2						
Graphite (1/8x2x3)	0.0000	0.0	0.0	1	1	5
SST (2x2x5)	0.0000	0.0	15.0	1	1	3
SST (1x2x6)	0.0000	0.0	30.0	2	1	1
SST (1/16x2x3)	0.1250	0.0	0.0	1	1	5
Graphite (1/8x2x3)	0.1875	0.0	0.0	1	1	5
SST (1/4x2x5)	0.3125	0.0	0.0	1	1	3
Graphite (1/8x2x3)	0.5625	0.0	0.0	1	1	5
SST (1/4x2x5)	0.6875	0.0	0.0	1	1	3
PANN (1/8x2x3)	0.9375	0.0	0.0	1	1	3
PANN (1/8x2x2)	0.9375	0.0	9.0	1	1	1
PANI (1/8x2x2)	0.9375	0.0	11.0	1	1	1
PANN (1/8x2x1)	0.9375	0.0	13.0	1	1	2
SST (1/4x2x5)	1.0625	0.0	0.0	1	1	3
Graphite (1/8x2x3)	1.3125	0.0	0.0	1	1	5
SST (1/4x2x5)	1.4375	0.0	0.0	1	1	3
Graphite (1/8x2x3)	1.6875	0.0	0.0	1	1	5
SST (1/16x2x3)	1.8125	0.0	0.0	1	1	5
Graphite (1/8x2x3)	1.8750	0.0	0.0	1	1	5
Wire Spring (2x2x1/16)	0.0000	0.0	36.0	1	1	1
Identification Number 3, Drawer Masters 1001-FS-3 and 1001-FM-3						
Graphite (1/8x2x3)	0.0000	0.0	0.0	1	1	5
SST (2x2x5)	0.0000	0.0	15.0	1	1	3
SST (1x2x6)	0.0000	0.0	30.0	2	1	1
SST (1/16x2x3)	0.1250	0.0	0.0	1	1	5
Graphite (1/8x2x3)	0.1875	0.0	0.0	1	1	5
SST (1/4x2x5)	0.3125	0.0	0.0	1	1	3
Graphite (1/8x2x3)	0.5625	0.0	0.0	1	1	5
SST (1/4x2x5)	0.6875	0.0	0.0	1	1	3
PANN (1/8x2x3)	0.9375	0.0	0.0	1	1	3
PANN (1/8x2x2)	0.9375	0.0	9.0	1	1	3
SST (1/4x2x5)	1.0625	0.0	0.0	1	1	3
Graphite (1/8x2x3)	1.3125	0.0	0.0	1	1	5
SST (1/4x2x5)	1.4375	0.0	0.0	1	1	3
Graphite (1/8x2x3)	1.6875	0.0	0.0	1	1	5
SST (1/16x2x3)	1.8125	0.0	0.0	1	1	5
Graphite (1/8x2x3)	1.8750	0.0	0.0	1	1	5
Wire Spring (2x2x1/16)	0.0000	0.0	36.0	1	1	1

Table 1.2 (cont'd). Core Drawer Plate Loading Descriptions.

Plate ID (size in inches)	Starting X location	Starting Y location	Starting Z location	X #	Y #	Z #
Identification Number 4, Drawer Masters 1001-FS-4 and 1001-FM-4						
Graphite (1/8x2x3)	0.0000	0.0	0.0	1	1	5
SST (2x2x5)	0.0000	0.0	15.0	1	1	3
SST (1x2x6)	0.0000	0.0	30.0	2	1	1
SST (1/16x2x3)	0.1250	0.0	0.0	1	1	5
Graphite (1/8x2x3)	0.1875	0.0	0.0	1	1	5
SST (1/4x2x5)	0.3125	0.0	0.0	1	1	3
Graphite (1/8x2x3)	0.5625	0.0	0.0	1	1	5
SST (1/4x2x5)	0.6875	0.0	0.0	1	1	3
PANN (1/8x2x3)	0.9375	0.0	0.0	1	1	3
PANI (1/8x2x3)	0.9375	0.0	9.0	1	1	2
SST (1/4x2x5)	1.0625	0.0	0.0	1	1	3
Graphite (1/8x2x3)	1.3125	0.0	0.0	1	1	5
SST (1/4x2x5)	1.4375	0.0	0.0	1	1	3
Graphite (1/8x2x3)	1.6875	0.0	0.0	1	1	5
SST (1/16x2x3)	1.8125	0.0	0.0	1	1	5
Graphite (1/8x2x3)	1.8750	0.0	0.0	1	1	5
Wire Spring (2x2x1/16)	0.0000	0.0	36.0	1	1	1
Identification Number 5, Drawer Masters 1001-FS-5 and 1001-FM-5						
Graphite (1/8x2x3)	0.0000	0.0	0.0	1	1	5
SST (2x2x5)	0.0000	0.0	15.0	1	1	3
SST (1x2x6)	0.0000	0.0	30.0	2	1	1
SST (1/16x2x3)	0.1250	0.0	0.0	1	1	5
Graphite (1/8x2x3)	0.1875	0.0	0.0	1	1	5
SST (1/4x2x5)	0.3125	0.0	0.0	1	1	3
Graphite (1/8x2x3)	0.5625	0.0	0.0	1	1	5
SST (1/4x2x5)	0.6875	0.0	0.0	1	1	3
PANN (1/8x2x3)	0.9375	0.0	0.0	1	1	5
SST (1/4x2x5)	1.0625	0.0	0.0	1	1	3
Graphite (1/8x2x3)	1.3125	0.0	0.0	1	1	5
SST (1/4x2x5)	1.4375	0.0	0.0	1	1	3
Graphite (1/8x2x3)	1.6875	0.0	0.0	1	1	5
SST (1/16x2x3)	1.8125	0.0	0.0	1	1	5
Graphite (1/8x2x3)	1.8750	0.0	0.0	1	1	5
Wire Spring (2x2x1/16)	0.0000	0.0	36.0	1	1	1

Table 1.2 (cont'd). Core Drawer Plate Loading Descriptions.

Plate ID (size in inches)	Starting X location	Starting Y location	Starting Z location	X #	Y #	Z #
Identification Number 7, Drawer Masters 1001-FS-7 and 1001-FM-7						
Graphite (1/8x2x3)	0.0000	0.0	0.0	1	1	5
SST (2x2x5)	0.0000	0.0	15.0	1	1	3
SST (1x2x6)	0.0000	0.0	30.0	2	1	1
SST (1/16x2x3)	0.1250	0.0	0.0	1	1	5
Graphite (1/8x2x3)	0.1875	0.0	0.0	1	1	5
SST (1/4x2x5)	0.3125	0.0	0.0	1	1	3
Graphite (1/8x2x3)	0.5625	0.0	0.0	1	1	5
SST (1/4x2x5)	0.6875	0.0	0.0	1	1	3
PANN (1/8x2x3)	0.9375	0.0	0.0	1	1	3
PANI (1/8x2x2)	0.9375	0.0	9.0	1	1	3
SST (1/4x2x5)	1.0625	0.0	0.0	1	1	3
Graphite (1/8x2x3)	1.3125	0.0	0.0	1	1	5
SST (1/4x2x5)	1.4375	0.0	0.0	1	1	3
Graphite (1/8x2x3)	1.6875	0.0	0.0	1	1	5
SST (1/16x2x3)	1.8125	0.0	0.0	1	1	5
Graphite (1/8x2x3)	1.8750	0.0	0.0	1	1	5
Wire Spring (2x2x1/16)	0.0000	0.0	36.0	1	1	1
Identification Number 11, Drawer Masters 1001-FS-11 (Core Thermocouple)						
Graphite (1/8x2x3)	0.0000	0.0	0.0	1	1	5
SST (1/16x2x3)	0.0000	0.0	15.0	1	1	7
SST (1x2x5)	0.0625	0.0	15.0	1	1	3
SST (1x2x6)	0.0625	0.0	30.0	1	1	1
SST (1/16x2x3)	0.1250	0.0	0.0	1	1	5
Graphite (1/8x2x3)	0.1875	0.0	0.0	1	1	5
SST (1/4x2x5)	0.3125	0.0	0.0	1	1	3
Graphite (1/8x2x3)	0.5625	0.0	0.0	1	1	5
SST (1/4x2x5)	0.6875	0.0	0.0	1	1	3
PANN (1/8x2x3)	0.9375	0.0	0.0	1	1	3
PANN (1/8x2x2)	0.9375	0.0	9.0	1	1	1
PANI (1/8x2x2)	0.9375	0.0	11.0	1	1	1
PANN (1/8x2x1)	0.9375	0.0	13.0	1	1	2
SST (1/8x1x2)	1.0625	0.0	0.0	1	1	18
SST (1/8x1/2x2)	1.0625	1.5	0.0	1	1	18
SST (1/8x2x3)	1.1875	0.0	0.0	1	1	5
SST (1/2x2x5)	1.1875	0.0	15.0	1	1	3
SST (1/2x2x6)	1.1875	0.0	30.0	1	1	1
Graphite (1/8x2x3)	1.3125	0.0	0.0	1	1	5

Table 1.2 (cont'd). Core Drawer Plate Loading Descriptions.

Plate ID (size in inches)	Starting X location	Starting Y location	Starting Z location	X #	Y #	Z #
Identification Number 11, Drawer Masters 1001-FS-11 (Core Thermocouple) (cont'd)						
SST (1/4x2x5)	1.4375	0.0	0.0	1	1	3
Graphite (1/8x2x3)	1.6875	0.0	0.0	1	1	5
SST (1/4x2x5)	1.6875	0.0	15.0	1	1	3
SST (1/4x2x6)	1.6875	0.0	30.0	1	1	1
SST (1/16x2x3)	1.8125	0.0	0.0	1	1	5
Graphite (1/8x2x3)	1.8750	0.0	0.0	1	1	5
SST (1/16x2x3)	1.9375	0.0	15.0	1	1	7
Wire Spring (2x2x1/16)	0.0000	0.0	36.0	1	1	1
Identification Number 11, Drawer Master 1001-FM-11 (Core Thermocouple)						
Graphite (1/8x2x3)	0.0000	0.0	0.0	1	1	5
SST (1/16x2x3)	0.0000	0.0	15.0	1	1	7
SST (1x2x5)	0.0625	0.0	15.0	1	1	3
SST (1x2x6)	0.0625	0.0	30.0	1	1	1
SST (1/16x2x3)	0.1250	0.0	0.0	1	1	5
Graphite (1/8x2x3)	0.1875	0.0	0.0	1	1	5
SST (1/4x2x5)	0.3125	0.0	0.0	1	1	3
Graphite (1/8x2x3)	0.5625	0.0	0.0	1	1	5
SST (1/4x2x5)	0.6875	0.0	0.0	1	1	3
PANN (1/8x2x3)	0.9375	0.0	0.0	1	1	3
PANN (1/8x2x2)	0.9375	0.0	9.0	1	1	1
PANI (1/8x2x2)	0.9375	0.0	11.0	1	1	1
PANN (1/8x2x1)	0.9375	0.0	13.0	1	1	2
SST (1/8x1x2)	1.0625	0.0	0.0	1	1	18
SST (1/8x1/2x2)	1.0625	1.5	0.0	1	1	18
SST (1/8x2x3)	1.1875	0.0	0.0	1	1	5
SST (1/2x2x5)	1.1875	0.0	15.0	1	1	3
SST (1/2x2x6)	1.1875	0.0	30.0	1	1	1
Graphite (1/8x2x3)	1.3125	0.0	0.0	1	1	5
SST (1/4x2x5)	1.4375	0.0	0.0	1	1	3
Graphite (1/8x2x3)	1.6875	0.0	0.0	1	1	5
SST (1/4x2x5)	1.6875	0.0	15.0	1	1	3
SST (1/4x2x6)	1.6875	0.0	30.0	1	1	1
SST (1/16x2x3)	1.8125	0.0	0.0	1	1	5
Graphite (1/8x2x3)	1.8750	0.0	0.0	1	1	5
SST (1/16x2x3)	1.9375	0.0	15.0	1	1	7
Wire Spring (2x2x1/16)	0.0000	0.0	36.0	1	1	1

Table 1.2 (cont'd). Core Drawer Plate Loading Descriptions.

Plate ID (size in inches)	Starting X location	Starting Y location	Starting Z location	X #	Y #	Z #
Identification Number 91, Drawer Master 1001-FS-10L (Core PSR)						
PSR Guide Tube (1/2x2x1)	0.0000	0.0	0.0	1	1	1
PSR (3/8x1.94x24)	0.0000	0.0	30.0	1	1	1
SST (1/16x2x3)	0.5000	0.0	0.0	1	1	5
SST (1/2x2x5)	0.5000	0.0	15.0	1	1	3
SST (1/2x2x6)	0.5000	0.0	30.0	1	1	1
Graphite (1/8x2x3)	0.5625	0.0	0.0	1	1	5
SST (1/4x2x5)	0.6875	0.0	0.0	1	1	3
PANN (1/8x2x3)	0.9375	0.0	0.0	1	1	5
SST (1x2x5)	1.0000	0.0	15.0	1	1	3
SST (1x2x6)	1.0000	0.0	30.0	1	1	1
SST (1/4x2x5)	1.0625	0.0	0.0	1	1	3
Graphite (1/8x2x3)	1.3125	0.0	0.0	1	1	5
SST (1/4x2x5)	1.4375	0.0	0.0	1	1	3
Graphite (1/8x2x3)	1.6875	0.0	0.0	1	1	5
SST (1/16x2x3)	1.8125	0.0	0.0	1	1	5
Graphite (1/8x2x3)	1.8750	0.0	0.0	1	1	5
Identification Number 92, Drawer Master 1001-FS-10R (Core PSR)						
Graphite (1/8x2x3)	0.0000	0.0	0.0	1	1	5
SST (1x2x5)	0.0000	0.0	15.0	1	1	3
SST (1x2x6)	0.0000	0.0	30.0	1	1	1
SST (1/16x2x3)	0.1250	0.0	0.0	1	1	5
Graphite (1/8x2x3)	0.1875	0.0	0.0	1	1	5
SST (1/4x2x5)	0.3125	0.0	0.0	1	1	3
Graphite (1/8x2x3)	0.5625	0.0	0.0	1	1	5
SST (1/4x2x5)	0.6875	0.0	0.0	1	1	3
PANN (1/8x2x3)	0.9375	0.0	0.0	1	1	5
SST (1/2x2x5)	1.0000	0.0	15.0	1	1	3
SST (1/2x2x6)	1.0000	0.0	30.0	1	1	1
SST (1/4x2x5)	1.0625	0.0	0.0	1	1	3
Graphite (1/8x2x3)	1.3125	0.0	0.0	1	1	5
SST (1/16x2x3)	1.4375	0.0	0.0	1	1	5
PSR Guide Tube (1/2x2x1)	1.5000	0.0	0.0	1	1	1
PSR (3/8x1.94x24)	1.5000	0.0	30.0	1	1	1

Table 1.2 (cont'd). Core Drawer Plate Loading Descriptions.

Plate ID (size in inches)	Starting X location	Starting Y location	Starting Z location	X #	Y #	Z #
Identification Number 91, Drawer Master 1001-FM-10L (Core PSR)						
Graphite (1/8x2x3)	0.0000	0.0	0.0	1	1	5
SST (1x2x5)	0.0000	0.0	15.0	1	1	3
SST (1x2x6)	0.0000	0.0	30.0	1	1	1
SST (1/16x2x3)	0.1250	0.0	0.0	1	1	5
Graphite (1/8x2x3)	0.1875	0.0	0.0	1	1	5
SST (1/4x2x5)	0.3125	0.0	0.0	1	1	3
Graphite (1/8x2x3)	0.5625	0.0	0.0	1	1	5
SST (1/4x2x5)	0.6875	0.0	0.0	1	1	3
PANN (1/8x2x3)	0.9375	0.0	0.0	1	1	5
SST (1/2x2x5)	1.0000	0.0	15.0	1	1	3
SST (1/2x2x6)	1.0000	0.0	30.0	1	1	1
SST (1/4x2x5)	1.0625	0.0	0.0	1	1	3
Graphite (1/8x2x3)	1.3125	0.0	0.0	1	1	5
SST (1/16x2x3)	1.4375	0.0	0.0	1	1	5
PSR (3/8x1.94x24)	1.5000	0.0	30.0	1	1	1
PSR Guide Tube (1/2x2x1)	1.5000	0.0	0.0	1	1	1
Identification Number 92, Drawer Master 1001-FM-10R (Core PSR)						
PSR Guide Tube (1/2x2x1)	0.0000	0.0	0.0	1	1	1
PSR (3/8x1.94x24)	0.0000	0.0	30.0	1	1	1
SST (1/16x2x3)	0.5000	0.0	0.0	1	1	5
SST (1/2x2x5)	0.5000	0.0	15.0	1	1	3
SST (1/2x2x6)	0.5000	0.0	30.0	1	1	1
Graphite (1/8x2x3)	0.5625	0.0	0.0	1	1	5
SST (1/4x2x5)	0.6875	0.0	0.0	1	1	3
PANN (1/8x2x3)	0.9375	0.0	0.0	1	1	5
SST (1x2x5)	1.0000	0.0	15.0	1	1	3
SST (1x2x6)	1.0000	0.0	30.0	1	1	1
SST (1/4x2x5)	1.0625	0.0	0.0	1	1	3
Graphite (1/8x2x3)	1.3125	0.0	0.0	1	1	5
SST (1/4x2x5)	1.4375	0.0	0.0	1	1	3
Graphite (1/8x2x3)	1.6875	0.0	0.0	1	1	5
SST (1/16x2x3)	1.8125	0.0	0.0	1	1	5
Graphite (1/8x2x3)	1.8750	0.0	0.0	1	1	5

Table 1.3. Radial Reflector Drawer Plate Loading Descriptions.

Plate ID (size in inches)	Starting X location	Starting Y location	Starting Z location	X #	Y #	Z #
Identification Number 101, Drawer Masters 1010-FS-1 and 1010-FM-1						
SST (1x2x6)	0.0	0.0	0.0	2	1	6
Wire Spring (2x2x1/16)	0.0	0.0	36.0	1	1	1
Identification Number 102, Drawer Masters 1010-FS-2 and 1010-FM-2						
SST (2x2x12)	0.0	0.0	0.0	1	1	2
SST (1x2x6)	0.0	0.0	24.0	2	1	2
Wire Spring (2x2x1/16)	0.0	0.0	36.0	1	1	1
Identification Number 103, Drawer Masters 1010-FS-3 and 1010-FM-3						
SST (2x2x6)	0.0	0.0	0.0	1	1	6
Wire Spring (2x2x1/16)	0.0	0.0	36.0	1	1	1
Identification Number 104, Drawer Masters 1010-FS-4 and 1010-FM-4						
SST (1/4x2x2)	0.0	0.0	0.0	8	1	18
Wire Spring (2x2x1/16)	0.0	0.0	36.0	1	1	1
Identification Number 191, Drawer Master 1010-FS-10L (SST Reflector PSR)						
PSR Guide Tube (1/2x2x1)	0.0	0.0	0.0	1	1	1
PSR (3/8x1.94x24)	0.0	0.0	30.0	1	1	1
SST (1/2x2x6)	0.5	0.0	0.0	1	1	6
SST (1x2x6)	1.0	0.0	0.0	1	1	6
Identification Number 192, Drawer Master 1010-FS-10R (SST Reflector PSR)						
SST (1x2x6)	0.0	0.0	0.0	1	1	6
SST (1/2x2x6)	1.0	0.0	0.0	1	1	6
PSR (3/8x1.94x24)	1.5	0.0	30.0	1	1	1
PSR Guide Tube (1/2x2x1)	1.5	0.0	0.0	1	1	1
Identification Number 191, Drawer Master 1010-FM-10L (SST Reflector PSR)						
SST (1x2x6)	0.0	0.0	0.0	1	1	6
SST (1/2x2x6)	1.0	0.0	0.0	1	1	6
PSR (3/8x1.94x24)	1.5	0.0	30.0	1	1	1
PSR Guide Tube (1/2x2x1)	1.5	0.0	0.0	1	1	1
Identification Number 192, Drawer Master 1010-FM-10R (SST Reflector PSR)						
PSR Guide Tube (1/2x2x1)	0.0	0.0	0.0	1	1	1
PSR (3/8x1.94x24)	0.0	0.0	30.0	1	1	1
SST (1/2x2x6)	0.5	0.0	0.0	1	1	6
SST (1x2x6)	1.0	0.0	0.0	1	1	6
Identification Number 111, Drawer Master 1010-FS-11 (SST Reflector Source)						
SST (1x2x6)	0.0	0.0	0.00	1	1	4
SST (1x2x1/8)	0.0	0.0	24.00	1	1	2
SST (1x2x1/16)	0.0	0.0	24.25	1	1	1
SST (1x2x5)	1.0	0.0	0.00	1	1	1

Table 1.3 (cont'd). Radial Reflector Drawer Plate Loading Descriptions.

Plate ID (size in inches)	Starting X location	Starting Y location	Starting Z location	X #	Y #	Z #
Identification Number 111, Drawer Master 1010-FS-11 (cont'd)						
SST (1x1/8x2)	1.0	0.0	5.00	1	4	9
SST (1x1/8x1)	1.0	0.0	23.00	1	4	1
SST (1x1/2x1/8)	1.0	0.0	24.00	1	1	2
SST (1x1/2x1/16)	1.0	0.0	24.25	1	1	1
Identification Number 111, Drawer Master 1010-FM-11 (SST Reflector Source)						
SST (1x2x5)	0.0	0.0	0.00	1	1	1
SST (1x1/8x2)	0.0	0.0	5.00	1	4	9
SST (1x1/8x1)	0.0	0.0	23.00	1	4	1
SST (1x1/2x1/8)	0.0	0.0	24.00	1	1	2
SST (1x1/2x1/16)	0.0	0.0	24.25	1	1	1
SST (1x2x6)	1.0	0.0	0.00	1	1	4
SST (1x2x1/8)	1.0	0.0	24.00	1	1	2
SST (1x2x1/16)	1.0	0.0	24.25	1	1	1
Identification Symbol P, Drawer Master 1030-BS-1 (SST Reflector Source)						
SST (1x2x6)	0.0	0.0	0.0	1	1	3
SST (1x2x5)	0.0	0.0	18.0	1	1	1
SST (1x2x1/8)	0.0	0.0	23.0	1	1	1
SST (1x1/8x2)	1.0	0.0	0.0	1	4	11
SST (1x1/8x1)	1.0	0.0	22.0	1	4	1
SST (1x1/2x1/8)	1.0	0.0	23.0	1	1	1
Identification Symbol Q, Drawer Master 1030-BM-1 (SST Reflector Source)						
SST (1x1/8x2)	0.0	0.0	0.0	1	4	11
SST (1x1/8x1)	0.0	0.0	22.0	1	4	1
SST (1x1/2x1/8)	0.0	0.0	23.0	1	1	1
SST (1x2x6)	1.0	0.0	0.0	1	1	3
SST (1x2x5)	1.0	0.0	18.0	1	1	1
SST (1x2x1/8)	1.0	0.0	23.0	1	1	1
Identification Number 201, Drawer Masters 1020-FS-1 and 1020-FM-1						
FE (1x2x36)	0.0	0.0	0.0	2	1	1
Identification Number 202, Drawer Masters 1020-FS-2 and 1020-FM-2						
FE (2x2x36)	0.0	0.0	0.0	1	1	1

A two-dimensional diagram of drawer master 1001-FS-2 (identified in the matrix loading maps by the symbol "2") is shown in Figure 1-8. This is an XZ view, i.e., looking down at the top of the drawer, and shows the columns of plates. (The drawer itself is not shown.) The origin of the drawer master coordinate system is at the front lower left corner of the space inside the drawer, which is near the upper left corner of the figure. The X axis is along the drawer width and is divided in eighth-inch units from zero to two inches (16 1/8-inch units). The Z axis is along the drawer length and goes from zero to 36 inches in inch units.[a] The Y axis is transverse to the page, pointing towards the viewer, and the range encompassing the plate loading is from zero to two inches. The plates being viewed are 2 inches tall, unless there is a note indicating otherwise.

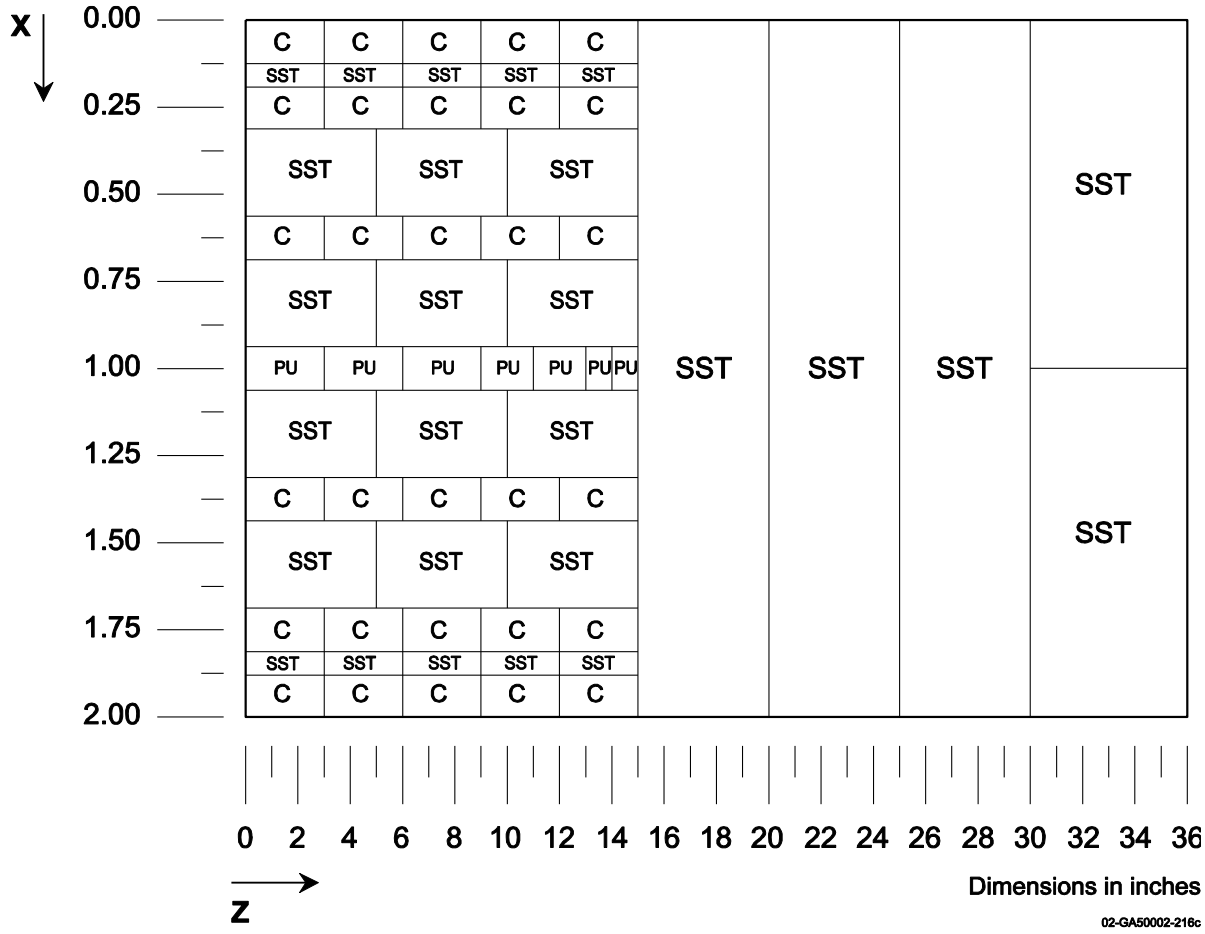

Figure 1-8. Diagram for Normal Core Drawer Master 1001-FS-2.

We begin by observing from Figure 1-8 that the first column is made of five 1/8 x 2 x 3-inch plates of graphite. Turning to Table 1.2, the first plate in master 1001-FS-2 indeed is shown to be 1/8 x 2 x 3-inch graphite; the first column of the table gives two pieces of information, a plate ID, which corresponds to the material description given in Section 1.3, and the X, Y, and Z dimensions of the plate. The beginning of the

[a] Note that the coordinate convention for ZPR assemblies is unusual in that the Z direction is horizontal, not vertical.

plate ID should give an approximate indication of the plate material (e.g., FE is iron, SST is stainless steel, PANN and PANI are steel clad Pu/1.1% Al metal fuel). The remaining columns of each table give the positions of the plates within the drawer. The second through fourth columns give the X, Y, and Z coordinates of the front lower left corner of a block of contiguous plates of this type. In this case, that position is seen to be the origin of the drawer coordinates, again consistent with Figure 1-8. The last three columns describe whether there is a single plate or a contiguous block of plates of this type. In this case, the block is 1 wide in X, 1 tall in Y, and 5 long in Z, i.e., there is one column consisting of five graphite plates. Figure 1-8 shows this first 15-inch region is followed by a 21-inch long steel region consisting of three 2 x 2 x 5-inch plates of stainless steel followed by two 1 x 2 x 6-inch plates of stainless steel. This is consistent with the next two entries in Table 1.2 that indicate three 5-inch thick steel plates beginning (axially) at 15 inches followed by a pair of 6-inch thick steel plates (side by side or 2 wide in X) beginning (axially) at 30 inches.

Moving now to the next column of plates in Master 1001-FS-2, it can be seen from Figure 1-8 that it is a 1/16-inch-wide column of stainless steel spanning the first 15 inches of the drawer, composed of 5 plates that are each 1/16 x 2 x 3 inches. Returning to Table 1.2, the fourth line for 1001-FS-2 shows these five steel plates in a column, starting at coordinates (0.125,0,0), that is 1 wide in X, 1 tall in Y, and 5 long in Z. In the next line there is a block of five 1/8 x 2 x 3-inch plates of graphite. This 1/8-inch thick column of graphite, starting at coordinates (0.1875,0,0), is 1 wide in X, 1 tall in Y, and 5 long in Z. (That is, the third column is built in the same manner as the first column.) Each successive line in Table 1.2 describes the next column of materials that fill the first 15-inch region in the drawer. The final entry in Table 1.2 for Master 1001-FS-2 indicates the wire spring that is placed behind the 36-inch long plate-filled portion of the drawer – spanning the width of the drawer and filling the remaining axial gap in the 36.252-inch long drawer, keeping the plate loading pressed fully to the front of the drawer.

Another potential point of confusion should be addressed, namely a difference between the convention for identifying matrix positions in the two halves and the convention for viewing drawer masters in the two halves. It was noted in Section 1.2.1 that, for both halves, the matrix column number (essentially the X coordinate) is counted from the left when looking from the movable half towards the stationary half. In contrast, the origin of the drawer master coordinates is at the left edge of the plates when looking from the matrix interface towards the matrix half that contains the drawer. To see how this works, compare the description of stationary-half drawer master 1001-FS-10R in Table 1.2 with the description of movable-half drawer master 1001-FM-10R in Table 1.2. The PSR guide tube is at the right edge in the stationary-half master and at the left edge in the movable-half master, yet these two (and the remaining) columns would align when the halves were brought together if these masters were in corresponding matrix positions, say S-26/32 and M-26/32.

A few dimension details for the PSRs were not given in Section 1.2.1 or in the tables. The stainless steel clad wall of a PSR was 0.032 inches thick, except for the front end cap, which was 0.125 inches thick. The wall thickness of the PSR guide tube was also 0.032 inches.

The section that follows offers a broader interpretation of the loading data. It is an attempt to describe the characteristics of each region of the assembly.

1.2.3 Characteristics of the Assembly Regions - We begin by observing some more characteristics of the drawer masters described in Tables 1.1 – 1.3. The half-height of the core is (nominally) 15 inches. Note that the discussion given in this section of the axial regions of the assembly refers to the nominal dimensions of the plates. The physical location of these plates in the assembly is also determined by the drawer front and/or back thicknesses. For example, fuel plates loaded in the first 15 inches of the core are displaced from the axial midplane by the thickness of the drawer front (0.032 inches).

The core matrix locations with non-standard drawer masters were the eight PSR positions (4 per half in the core periphery) and the six thermocouple drawers (3 per half). The loading of these drawer types differed only slightly from the standard core drawers. In the case of the PSR positions, the drawers themselves were different. The PSR drawers were narrow (nominally 1.5 inches wide and 36.252 inches long) and were not perforated. In these matrix locations, there was a thin steel sleeve or guide tube filling the remaining 0.5 inch, creating a channel in which the PSR (boron poison safety rod) could travel for insertion into the core. Recall that the PSRs were not in the core region during the criticality measurement. The inside loading of the control drawers was identical to the core drawer loading for the remaining 1.5 inches of the core unit cell. In the thermocouple drawers, the steel column adjacent to the central fuel column was modified to use 1/8 x 1 x 2 inch steel plates below the thermocouple leads and 1/8 x 1/2 x 2 inch steel plates above the thermocouple leads. That is, insertion of the thermocouples entailed only a small removal of steel to allow insertion of the thermocouples. Thus, overall, the core loading was quite uniform. In summary, there were only minor perturbations in the core loading; these small loading variations are known; and they can be modeled.

The axial reflector region was built by filling the final 21 inches of the 36-inch drawers with stainless steel blocks (see Figure 1-8). This region had the same two kinds of drawer master perturbations as the core. The thermocouple drawer loading included a small gap to accommodate the thermocouple wires. The PSR drawers were completely filled with stainless steel over the 21 inch extent of the axial reflector region. During the criticality measurement the associated guide tube was empty in the first 15 inches of the axial reflector but occupied by the PSR beyond there.

The radial reflector region was built by filling the stainless steel drawers completely with stainless steel blocks. The core was surrounded by these steel-filled drawers to form a steel reflector region that was eight drawers thick (or ~17.4 inches). There were eight PSR positions (4 per half) located in the radial reflector region in matrix locations adjacent to the core region. The PSR drawers were completely filled with stainless steel over their full 36 inch length. During the criticality measurement the associated guide tube was empty in the first 30 inches but occupied by the PSR beyond there. There was only one further perturbation in the loading of the radial reflector. In one matrix location per half, the reflector loading (SST) spanned only half the width of the drawer. In the other half-width of the drawer, four 1/8-inch thick stainless steel plates were stacked on their sides, only partially filling this portion of the drawer. This produced a 1-inch-wide gap axially in these matrix locations (S/M 33/25) that allowed the insertion of a neutron source. These were also the only matrix locations that contained front/back drawer combinations. Overall, the stainless steel radial reflector was quite uniform.

This steel reflector region was then surrounded by an iron radial reflector region that was 3 drawers thick (or ~6.5 inches). These iron reflector drawers were completely filled with a 36-inch loading of iron blocks.

It may be noted that only one of the drawer master diagrams of the ZPR-6/10 assembly has been included herein (Figure 1-8) to aid in visualizing these unit cells. Inclusion of these diagrams is redundant, since all the drawer masters included in this assembly are completely specified by the information in Tables 1.2 and 1.3.

In summary, ZPR-6 Assembly 10 had a very clean and uniform core built with a simple Pu/C/SST core unit cell. This core region was then well isolated by thick solid radial and axial reflectors. The simplicity and uniformity of this assembly was intended to make it a clean benchmark assembly.

1.3 Description of Material Data

The composition data here were taken from working documents that are referred to informally as "hot constants memos". The original documentation on most of the inventory used in ZPR-6/10 has been lost, but the hot constants memos are available. These memos give average composition by batch or lot, but not uncertainties. The issue of estimating composition uncertainties is addressed in Section 2. The compositions of the plutonium plates were taken from the Illinois hot constants memo,[a] which is the most reliable source of information on these materials. The ZPPR (Zero Power Physics Reactor) hot constants memo[b] was used for all other ZPR-6/10 components that it describes because this memo has the most complete and accurate description of trace elements.

Two types of Pu/Al plates were used in Assembly 10. These two plate types were referred to as PANN and PANI, which indicated Pu/Al fuel without nickel (i.e., No Nickel) and Pu/Al fuel with nickel (NI), respectively. The nominal compositions of the plates vary only by an additional nickel coating on the plutonium for the PANI plates. Both plate types were clad in stainless steel cans. Three different size PANN plates and two different PANI plates were used for this benchmark geometry. Fuel and clad masses and outer dimensions for these plates are given in Tables 1.4 and 1.5. The stainless steel cans for the PANI and PANN plates are 0.012 in. (front), 0.058 in. (back), 0.020 in. (sides), and 0.1175 in. (top and bottom). The additional nickel coating on the PANI plates amounts to only a few mils on the Pu core dimensions and for simplicity the Ni was merged in with the cladding. (The overall can dimensions were modeled the same for both the PANN and PANI fuel plates. This simplification is discussed in Section 2.) The small differences between the PANN and PANI plates are evident from Tables 1.4 and 1.5. Each Pu/Al fuel plate was weighed before and after cladding, and these masses were recorded in a database. The masses shown in Tables 1.4 and 1.5 are the average values for the given plate type and size, as derived from this database. Similarly, samples from each melt were analyzed when the fuel was cast, and these data were used to derive the aluminum and Pu isotopic mass distributions in Table 1.4.

[a] W. R. Robinson, Applied Physics Division Reactor Materials Inventory Manual–Chapter 3, A0033-1000-SE-01, July 1978.
[b] T. S. Huntsman, ZPPR Materials Compositions, July 1983.

Table 1.4. Plutonium Fuel Compositions.

Plate ID	Nominal Size[(a)] (inches)	^{239}Pu Mass(g)	^{240}Pu Mass(g)	^{241}Pu Mass[(b)] (g)	^{242}Pu Mass(g)	^{241}Am Mass[(a)] (g)	Al Mass (g)
PANN (1/8x2x1)	0.125 x 2.00 x 1.00	30.69920	1.45890	0.05560	0.00000	0.06660	0.36470
PANN (1/8x2x2)	0.125 x 2.00 x 2.00	65.59241	3.12170	0.12000	0.00000	0.14349	0.77030
PANN (1/8x2x3)	0.125 x 2.00 x 3.00	98.98241	4.71610	0.20760	0.00490	0.24820	1.15839
PANI (1/8x2x2)	0.125 x 2.00 x 2.00	65.35170	3.05550	0.14000	0.03010	0.17470	0.82050
PANI (1/8x2x3)	0.125 x 2.00 x 3.00	98.81351	4.68210	0.18370	0.06000	0.22910	1.25080

(a) Outer clad dimensions.
(b) Masses of ^{241}Pu and ^{241}Am correspond to January 1, 1977.

Table 1.5. Stainless Steel Clad Mass and Compositions for Pu/Al Fuel.

Plate ID	Clad Mass(g)	Composition wt. %									
		C	Si	P	S	Cr	Mn	Fe	Ni	Cu	Mo
PANN (1/8x2x1)	8.78	0.07	0.48	0.02	0.02	18.45	1.71	69.60	8.88	0.27	0.32
PANN (1/8x2x2)	16.80	0.07	0.48	0.02	0.02	18.45	1.73	69.70	8.93	0.28	0.32
PANN (1/8x2x3)	24.76	0.06	0.48	0.02	0.02	18.45	1.70	69.70	8.96	0.28	0.32
PANI (1/8x2x2)	20.21	0.06	0.43	0.02	0.02	16.37	1.51	61.84	19.22	0.25	0.28
PANI (1/8x2x3)	29.78	0.06	0.43	0.02	0.02	16.39	1.51	61.90	19.13	0.25	0.29

The mass and composition of the graphite plates used in the ZPR-6/10 are given in Table 1.6.

Table 1.6. Graphite Plate Compositions.

Plate ID	Nominal Size (inches)	Graphite Mass (g)	C Density[(a)] (g/cc)	C (wt.%)
Graphite (1/8x2x3)	0.125x2.00x3.00	20.04	1.63055	100.0

(a) Derived from mass and nominal dimensions.

The compositions of the iron blocks used in the iron radial reflector are given in Table 1.7.

Table 1.7. Iron Block Compositions.

Nominal Size (inches)	Mass (g)	Density[(a)] (g/cm^3)	C (wt.%)	Mn (wt.%)	Fe (wt.%)	P (wt.%)	S (wt.%)	Si (wt.%)
1 x 2 x 36	9200	7.78	0.10	0.50	99.31	0.013	0.024	0.024
2 x 2 x 36	18440	7.81	0.23	0.75	98.93	0.013	0.024	0.024

(a) derived from mass and nominal dimensions.

The compositions of the stainless steel plates are given in Table 1.8. All plate types have densities that vary by only a few percent and have about the same weight percentages of constituents (except for trace elements). These compositions are based on certificates provided by the vendors. In some cases all the plates of a given size came from a single procurement. More often, the inventory of a given plate size is the combination of several procurements and then the displayed composition is the average.

Table 1.8. Stainless Steel Plate Compositions.

Nominal Size (in)	Mass (g)	Density[(a)] (g/cm^3)	C (wt.%)	Si (wt.%)	P (wt.%)	S (wt.%)	Cr (wt.%)	Mn (wt.%)	Fe (wt.%)	Ni (wt.%)	Cu (wt.%)	Mo (wt.%)
1/16 x 1/2 x 1	3.79	7.40	0.06	0.20	0.03	0.02	18.32	1.55	70.51	8.51	0.20	0.25
1/16 x 2 x 1	15.78	7.70	0.06	0.20	0.03	0.02	18.32	1.55	70.51	8.51	0.20	0.25
1/16 x 2 x 3	45.80	7.45	0.06	0.20	0.03	0.02	18.32	1.55	70.51	8.51	0.20	0.25
1/8 x 1/2 x 1	7.58	7.40	0.06	0.20	0.03	0.02	18.32	1.55	70.51	8.51	0.20	0.25
1/8 x 1 x 1	15.29	7.70	0.06	0.20	0.03	0.02	18.32	1.55	70.51	8.51	0.20	0.25
1/8 x 1 x 2	30.89	7.54	0.06	0.20	0.03	0.02	18.32	1.55	70.51	8.51	0.20	0.25
1/8 x 1/2 x 2	15.26	7.45	0.06	0.20	0.03	0.02	18.32	1.55	70.51	8.51	0.20	0.25
1/8 x 2 x 3	93.39	7.60	0.06	0.20	0.03	0.02	18.32	1.55	70.51	8.51	0.20	0.25
1/4 x 2 x 2	127.6	7.78	0.06	0.20	0.03	0.02	18.32	1.55	70.51	8.51	0.20	0.25
1/4 x 2 x 5	320.0	7.81	0.06	0.20	0.03	0.02	18.32	1.55	70.51	8.51	0.20	0.25
1/4 x 2 x 6	369.4	7.51	0.05	0.27	0.03	0.04	18.60	1.52	70.50	8.66	0.20	0.42
1/2 x 2 x 5	628.3	7.67	0.07	0.54	0.03	0.03	18.28	1.79	70.11	9.14	0	0
1/2 x 2 x 6	753.3	7.66	0.07	0.54	0.03	0.03	18.28	1.79	70.11	9.14	0	0
1 x 2 x 5	1269	7.74	0.07	0.67	0.03	0.03	18.50	1.90	69.55	9.25	0	0
2 x 2 x 5	2578	7.87	0.06	0.57	0.04	0.02	18.40	1.99	69.65	9.27	0	0
1 x 2 x 6	1511	7.68	0.07	0.67	0.03	0.03	18.50	1.90	69.55	9.25	0	0
2 x 2 x 6	3024	7.69	0.06	0.57	0.04	0.02	18.40	1.99	69.65	9.27	0	0
2 x 2 x 12	6065	7.71	0.06	0.34	0.03	0.03	18.52	1.38	70.58	8.78	0.10	0.28

(a) derived from mass and nominal dimensions.

The tables giving the compositions of the remaining components present the information in a different form from that in earlier tables. The mass of each element is shown, rather than the total mass, total density and weight percent by isotope. The drawer is broken down into various walls or wall combinations. The second column gives the nominal dimensions in the order X × Y × Z (following the convention described in Section 1.2.2). Note that the masses given for the sides plus bottom are per inch of drawer length, not for the total drawer length.

Table 1.9 has the stainless steel drawer descriptions in this format. These drawers were made of Type 304 stainless steel. Some components were perforated to varying degrees while others had no holes. An example of perforations in a drawer front is shown in Figure 1-3. The control drawers not only were narrow, but also had a very thin (~ few mils) steel cover. (The mass of this thin cover is included in the side walls and bottom in the "as-built" modeling of this drawer for the VIM continuous-energy Monte Carlo code.[a])

Table 1.9. Stainless Steel Drawer Compositions.

Description	Nominal Size (inches)	C (g)	Si (g)	P (g)	S (g)	Cr (g)	Mn (g)	Fe (g)	Ni (g)	Cu (g)	Mo (g)
Control Drawer											
Side Walls[(a)] + Cover[(a)] + Bottom[(a)]	2x(.031x2x1) + 1.5x.031x1	0.015	0.137	0.007	0.001	4.018	0.386	15.602	1.848	0.057	0.046
Front	1.5 x 2 x .035	0.008	0.054	0.003	0.001	2.245	0.203	8.511	1.112	0.023	0.040
Back	1.5 x 2 x .031	0.011	0101	0.005	0.001	2.951	0.279	11.459	1.358	0.042	0.034
Core SST Drawer											
Side Walls[(a)] + Bottom[(a)]	2x(.031x2x1) + 2x.031x1	0.016	0.155	0.005	0.002	4.263	0.396	16.344	2.117	0.096	0.078
Front	2 x 2 x 0.31	0.008	0.076	0.002	0.001	2.099	0.196	8.047	1.042	0.047	0.038
Back	2 x 2 x 0.62	0.013	0.127	0.004	0.002	3.456	0.320	13.249	1.716	0.078	0.063
Reflector SST Drawer											
Side Walls[(a)] + Bottom[(a)]	2x(.031x2x1) + 2x.031x1	0.006	0.047	0.003	0.001	1.980	0.146	7.478	0.996	0.013	0.014
Front	2 x 2 x 0.36	0.015	0.045	0.003	0.001	2.892	0.104	13.337	0.454	0.017	0.020
Back	2 x 2 x 0.31	0.009	0.008	0.004	0.001	2.533	0.233	9.648	1.137	0.033	0.026

(a) Mass per inch of length.

[a] R. N. Blomquist, R. M. Lell and E. M. Gelbard, "VIM – A Continuous Energy Monte Carlo Code at ANL," A Review of the Theory and Application of Monte Carlo Methods, Proceedings of a Seminar-Workshop, Oak Ridge, TN, April 21-23, 1980, ORNL/RSIC-44, p. 31, August 1980.

The compositions of the various tubes and springs are given in Table 1.10. The only component that has a significant reactivity effect is the matrix tube. The masses for this and the other tube types are for a one-inch length, not the full length. The matrix tube masses for the first inch (at the matrix interface) were less than shown because there was a 0.313x0.687 inch notch in each side wall (to accommodate the tabs on the side walls of some drawers). The wire spring was used to compress the fuel plates toward the front of the drawer. A retainer spring was used at the back of each radial reflector.

Table 1.10. Matrix Tube, PSR Guide Tube, Source Tube, and Wire Spring Compositions.

Component	C (g)	Si (g)	P (g)	S (g)	Cr (g)	Mn (g)	Fe (g)	Ni (g)	Cu (g)	Mo (g)
Matrix Tube[(a)]	0.029	0.247	0.011	0.003	7.959	0.749	30.763	3.629	0.141	0.102
PSR Guide Tube[(a)]	0.012	0.093	0.006	0.002	3.925	0.289	14.824	1.975	0.026	0.028
Source Tube[(a)]	0.001	0.007	.001	.001	0.385	0.029	1.467	0.182	0.002	0.006
Wire Spring	0.049	0.0	0.0	0.0	0.084	0.008	0.325	0.042	0.004	0.0
Retainer Spring	0.097	0.0	0.0	0.0	0.0	0.0	9.862	0.0	0.0	0.0

(a) Mass per inch of length.

The only aspect of the PSR blade composition that has any significance for the criticality measurements is the mass of ^{10}B per unit length. With the PSRs fully withdrawn, as they were for the criticality measurements, even this strong neutron poison has almost no effect (see Section 2.2). The linear mass density, in grams of ^{10}B per inch, was different for each blade. It ranged from 5.67 to 9.57 and the average value was 7.23 g/inch.

1.4 Temperature Data

The reported excess reactivity for ZPR-6/10 loading 24 was adjusted to a standard temperature of 25 °C by the experimenters. The isothermal temperature coefficient (determined to be a function of whether the cooling fans were on or off and of the reactor power level) was measured to be –4.82 Ih/°C.

1.5 Supplemental Experimental Measurements

A list of experiments performed in the Pu/C/SST Benchmark Assembly is given below. As noted in Section 1.1, this assembly was part of a program to resolve several long-standing discrepancies between calculated and experimental values for a number of integral parameters. Experiments were done to characterize its neutronics properties as thoroughly as possible. But the main emphasis was on experiments to measure the reactivity associated with small samples of fissile material, $ß_{eff}$, and capture in ^{238}U. None of the listed measurements, other than criticality, were made in Loading 24, but in Pu/C/SST Benchmark Assembly loadings so similar to Loading 24 that the results are directly applicable to it. Reference 1 is the only open-literature document that contains information about some of the experiments. Argonne National Laboratory internal memoranda exist that describe all the experiments.

Experiments performed in the Pu/C/SST Benchmark Assembly (ZPR-6/10):[a,b]

- Criticality.
- Kinetics parameters: $ß_{eff}$, ß/l, $ß_i$/ß, and $a_i\lambda_i$.
- Control rod calibrations (Comparison of Inverse Kinetics and Positive-Period Methods).
- Matrix Interface gap worth.
- Reaction rates in a central cavity.
- Reaction rates in the unit cell (f^{49}, f^{25}, f^{28}, and c^{28}).
- Reaction-rate axial and radial distributions (f^{49}, f^{25}, f^{28}, and c^{28}).
- Special Reaction Rate Measurements (Na and Au).
- ^{10}B and ^{235}U Track Exposure Measurements.
- Worth of Pu/DU/C Zone – Assembly 10Z -- (criticality, kinetics parameters; reaction rates and distributions).

[a] Private communication, R. B. Pond and R. A. Scharping, Argonne National Laboratory, February 1, 1982.
[b] Private communication, D. M. Smith, R. B. Bucher, and R. W. Schaefer, Argonne National Laboratory, October 19, 1983.

2.0 EVALUATION OF EXPERIMENTAL DATA

As noted in Section 1.1, there were several critical loadings in the ZPR 6/10 Benchmark Assembly program. Any one of them would provide about the same basic criticality-safety benchmark information, so the basis for selecting a particular loading for use here was the precision and accuracy with which the critical assembly could be described. The selected loading is ZPR 6 Assembly 10 Loading 24. A number of loading changes were made over a period of a month and then a loading nominally identical to Loading 24 was restored, with the designation Loading 37.

The uncertainties affecting criticality have been divided into three broad categories. They are uncertainties associated with 1) measurement technique, 2) geometry, and 3) compositions. Each category is considered in turn and then the combined experimental uncertainty is presented. Each uncertainty estimate is one standard deviation.

Reactivity effects of uncertainties in geometry were calculated for the as-built model of ZPR-6/10 Loading 24 using MCNP6 with ENDF/B-VII.0 data. Reactivity effects of uncertainties in material compositions were calculated with a deterministic model of the assembly. The BuildZPRModel[a] code was used to create a deterministic model that is equivalent to the as-built Monte Carlo model. MC^2-3[b] was used to generate ENDF/B-VII.0 cross sections for the calculations. The slab lattice capability in MC^2-3 accounts for the heterogeneous structure of each drawer. DIF3D-VARIANT[c] was used for the deterministic transport calculations. Various space-angle-energy approximations were tested. The final calculations used a spatial approximation consisting of a 6^{th} order flux, 4^{th} order source and 1^{st} order leakage approximation. The angular approximation used a P_3 flux and P_3 scattering kernel. The final calculations used 230 energy groups although limited sets of calculations were performed with 425 groups and 703 groups for test and verification purposes.

In cases where the change in k_{eff} might be too small to obtain accurately with the 10^{-7} k_{eff} convergence criterion, the atom density changes were scaled up to give about a 10^{-4} change in k_{eff} and the resulting Δk was then scaled down to the actual perturbation. A 10^{-4} k_{eff} change is small enough to be a first-order perturbation, which justifies the scaling. The uncertainties are put in units of $\%\Delta k$ (100 times the change in k_{eff}). For consistency in accounting, they are always displayed to four decimal places, even though that level of precision is not always justified on physical grounds.

2.1 Measurement Technique Uncertainties

The excess reactivity was measured in two ways. One was positive period measurements. Complications in interpreting these were nonlinearities in the detection system and changes in both the average temperature and the temperature distribution during the excursion. The other method was use of control rod worths that were obtained by the rod-drop inverse-kinetics technique. A number of determinations, each made using a different rod, gave similar results. Here again, variations in the distribution of temperatures throughout the assembly, for the same average of 16 thermocouples, complicate the interpretation.

A large number of measurements were made to understand, in as much detail as practical, the temperature effects in the assembly. For example, measurements were made with the cooling fans on, with fans off, with

[a] A. Mohamed and M. A. Smith, Argonne National Laboratory, Personal Communication, April 1, 2011.
[b] C. H. Lee and W. S. Yang, "MC^2-3: A Multigroup Cross Section Generation Code for Fast Reactor Analysis," ANL/NE-11-41, Argonne National Laboratory, January 2012.
[c] M. A. Smith, E. E. Lewis and E. R. Shemon, "DIF3D-VARIANT 11.0, A Decade of Updates," ANL/NE-14/1, Argonne National Laboratory, 2014.

very little fission power and with significant fission power. The results were all adjusted to the same matrix gap readout and to the same average temperature, 25º C. For Loading 24 the estimated excess reactivity ranged from 74 Ih to 79 Ih. Fewer measurements were made for Loading 37. Those values ranged from 80 Ih to 83 Ih and they are about 2.6 Ih higher than estimates made for Loading 24 by the corresponding approach, i.e., for the same set of conditions regarding cooling fans, reactor power level, etc. The 2.6 Ih difference is a measure of reproducibility limitations associated with the axial positions of drawers and plates (see Section 2.2) and with plate-to-plate composition variations (see Section 2.3). A reproducibility uncertainty is 2.6 Ih is reasonable for a ZPR-6 assembly and is consistent with estimates of reproducibility for other ZPR-6 and ZPR-9 assemblies such as the high ^{240}Pu ZPR-6/7 core (see MIX-COMP-FAST-005). This reproducibility uncertainty is negligible compared to some of the composition uncertainties for this assembly and would remain small for any realistic increase in the reproducibility uncertainty. Consequently, further effort to refine this uncertainty is not worthwhile.

For the purposes of this benchmark, it should be sufficient simply to use the midpoint of the entire 74-to-83 Ih range as the best estimate and to assume that this range corresponds to ±2σ. Accordingly, the estimated excess reactivity is 78.5 Ih and the 1σ uncertainty is ±2.3 Ih. This value is small compared to some of the composition uncertainties, so further effort to refine the uncertainty in the estimated excess reactivity is not warranted.

To convert from the natural measurement units of Ih to units of k_{eff} requires an accurate assessment of β_{eff}. The calculated conversion factor from Ih to units of k_{eff} for this assembly, obtained using ENDF/B-V cross section and delayed-neutron data, is 1141 Ih/%Δk. The family-dependent relative delayed neutron yields, $a_i = \beta_i/\beta$, and decay constants, λ_i, for each of six delayed neutron families were measured by fitting rod drop data using inverse kinetics. Using these results, and the calculated values of β_{eff} and prompt neutron lifetime, the conversion factor was estimated to be 1120 Ih/%Δk. This is approximately 2% lower than the estimate based on calculation alone. The main determinant of the conversion factor is β_{eff}. A measurement on ZPR-6/10 by the noise technique[1] yielded a β_{eff} value that is higher than the calculated one by 1.3% ± 2%. To be consistent with other ZPR benchmark evaluations, the calculated conversion factor of 1141 Ih/%Δk will be used and it will be assumed to be uncertain by 5%. Using that conversion factor, the measured excess reactivity is 0.0688% Δk with a measurement uncertainty of 0.0020% Δk. The uncertainty in the conversion factor applied to the excess reactivity leads to an additional uncertainty of 0.0034%Δk. The reproducibility uncertainty is 2.6 Ih or 0.0023%Δk.

2.2 Geometry Uncertainties

Because the matrix halves were not perfectly aligned, there was a small gap of variable width between the two halves of the assembly, even when the halves made contact at a point. The best estimate of the average residual gap at nominal full closure is 25 mils (0.635 mm), and an estimated upper bound is 50 mils (1.27 mm). The range from zero to this upper bound, i.e., the 0 – 50 mil range, is assumed to represent ±2σ or 4σ total. Consequently, 1σ is assumed to be 12.5 mil (50/4 mil).

The reactivity effect associated with these gap values can be determined from the measured gap coefficient. Excess reactivity was measured in ZPR-6/10 as a function of gap width. The results are nonlinear, with a larger-magnitude slope at larger gaps. For small gaps near nominal full closure, a linear fit yielded –263.0 ± 8.5 Ih/cm. A ±1σ gap uncertainty of 12.5 mils corresponds to 0.03175 cm, so the worth of the gap uncertainty is 8.35025 Ih (263.0 x 0.03175) with an associated uncertainty due to the linear fit of 0.26988 Ih (8.5 x 0.03175). Adding these two components in quadrature, the total gap worth uncertainty is 8.3546 Ih or

0.0073 %Δk, assuming a reactivity conversion factor of 1141 Ih/%Δk. Again based on this gap coefficient, increasing the experimental k_{eff} 0.0146 %Δk would account for omission of the estimated 25-mil gap from the model.

Besides the table gap, there are three issues regarding the exact location of materials. One such possibility is that the drawer fronts might not have been flush with the front edge of the matrix tubes. This component was minimized by ensuring the tabs on the drawer sides mated with notches in the matrix tubes. During drawer loading and unloading, care was taken to make the drawers flush with the matrix surface. The second issue is the possibility that the plate columns might not have been all the way forward against the drawer front. This problem was minimized by following the drawer loading procedure and by using springs to hold the plates in a fixed position. Both of these two issues are assumed covered by the table gap uncertainty.

The third issue is deviations from nominal dimensions for plates, drawers, and matrix tubes. Deviations in the dimensions that affect the precise X and Y positions of materials in the unit cell are too small to impact k_{eff} significantly. The dimensions that determine the volumes over which the material masses are distributed can have an effect. The plate lengths and drawer front thickness affect the axial positions of materials, similar to the interface gap effect. It is estimated that the collective uncertainty in these dimensions is ±10 mils (0.25 mm). Using the gap coefficient as a measure of the reactivity effect yields a k_{eff} uncertainty contribution of ±0.0058 %Δk. A deviation from the nominal average spacing between matrix tubes, discussed next, also would affect region volumes.

The average matrix tube pitch was measured for the expanded ZPR-6 matrix to be 2.177 inches. The measured pitch is assumed to be uncertain by 1 mil (1σ). The effect of increasing or decreasing the pitch by 1 mil was computed with the as-built Monte Carlo model. The matrix tube pitch was increased or decreased by 1 mil, and the atom density for the matrix tubes was adjusted to conserve matrix tube mass. The dimensions and compositions of the drawers and their contents are not affected by the change in matrix tube pitch.

The effect of changing the matrix tube pitch by 1 mil in each direction is ±0.0370 %Δk per mil (0.00254 cm). The magnitude of this result is taken to be the pitch contribution to the k_{eff} uncertainty. This coefficient also indicates that increasing the experimental k_{eff} by 0.0740 %Δk would compensate for use in the model of a 2.175-inch square pitch, which is the traditional value used in ZPR analyses.

The PSR control rods are another source of geometric uncertainty. Because the measured excess reactivity corresponds to having the leading edge of all the poison blades deep into the axial reflector, 30 in. from the core, they should have very little impact. In fact, the PSR blades were omitted entirely from the as-built model, except in one test calculation. The Monte Carlo-calculated effect of the PSR blades is within the statistical uncertainty, -0.00062 ±0.00093%Δk. But it was believed that the effect actually is small compared to this statistical uncertainty. This was confirmed by modifying a TWODANT[a] model of the RZ benchmark to have an annular region with boron, representing the smeared ring of PSR blades. Smearing a ring of boron control rods in this manner is known to over-estimate the rod worth because self shielding is reduced. The TWODANT result is -0.0003 %Δk. Because this result is so small, the PSR blades were omitted from the models and are accounted for by including this result as an uncertainty.

Room return of neutrons to the assembly is the last geometric source of uncertainty. The assembly description encompasses only a small fraction of the empty matrix beyond the matrix tubes containing plate material. The effects of room return were computed with the as-built Monte Carlo model. The as-built model was expanded to include the full matrix, the table and support structure around the matrix tubes, and

[a] R. E. Alcouffe, F. W. Brinkley, D. R. Marr and R. D. O'Dell, "Users's Guide for TWODANT: A Code Package for Two-Dimensional, Diffusion-Accelerated Neutral-Particle Transport," LA-10049-M, Revised February 1, 1990.

the room containing ZPR-6. The computed worth of adding room return was -0.0028 ± 0.0026%Δk. Adding room return must increase reactivity, so the computed worth is just an artifact of the Monte Carlo calculation. The worth of room return is negligible, and the associated uncertainty is 0.0026%Δk.

2.3 Composition Uncertainties

A bit of history about the materials inventory records is needed to appreciate the extent and limitations of the information available on the compositions used in ZPR-6/10. The material inventory for Argonne's ZPR facilities was accumulated over a period of more than three decades, starting in the mid-1950s. The procurement acceptance process required thorough documentation on dimensions, masses, compositions, etc. of the various core components. Information needed for day-to-day operations was extracted and compiled in working documents known informally as "hot constants memos." These memos give batch or lot average values of dimensions, masses, and weight percents of constituents but no uncertainties. The original documentation on much of the inventory used in ZPR-6/10 is no longer available, but the hot constants documents are available. Consequently, indirect evidence and estimates were used to quantify many of the composition uncertainties. Compositions given in these hot constants documents are used directly. That is, weight fractions are not adjusted or renormalized to sum to 100%.

The composition uncertainty for a component is treated in two parts: the uncertainty in total mass and the uncertainty in the weight percents of the constituents. Since these two sources of uncertainty are independent, they are added in quadrature. The reactivity effect of the composition uncertainty was determined by computing the change in the k_{eff} using the DIF3D-VARIANT deterministic model of the benchmark. In some cases sensitivity coefficients computed with this model were used, and in other cases the specific perturbation was calculated explicitly.

The details of the mass measurements are unknown. For the plates and most of the drawers it is assumed that measurements of masses were within 0.01 g of actual value for plates of up to tens of grams and within 1 g for larger plates weighing kilograms, i.e., the uncertainty in weighing was 0.1%. The working standard used to calibrate the scale is taken to have an uncertainty of 0.05%, which is a systematic uncertainty. The uncertainty in weighing could be statistical, but since no details of the process are available, we assume this to be a systematic uncertainty, making a total uncertainty in mass of 0.15%. This mass uncertainty assumption is made for items where no specific mass uncertainty information is available.

The materials that could contribute in a significant way to the composition uncertainties are: the Pu/Al fuel plates, the graphite plates, the stainless steel plates, the stainless steel drawers, and the stainless steel matrix tubes. Masses and compositions for all of these materials are known reasonably well.

The uncertainty in the total plutonium mass in the Pu-Al plates was computed to be 0.0720% based on analysis of a database of mass and composition information for the Pu-Al plates. With the exception of the ^{241}Pu decay uncertainty, all relative uncertainties in mass, composition and isotopics for the Pu-Al plates were derived from the same database. Increasing the plutonium (plus americium) mass in the Pu-Al plates by this amount in the TWODANT model increased k_{eff} by 0.0302 %Δk.

The relative uncertainty in the ^{239}Pu weight percent was computed to be 0.0256% for the Pu-Al plates. In the DIF3D-VARIANT model, the ^{239}Pu concentration was increased by this amount and mass was preserved by decreasing just the ^{240}Pu concentration (a simplification justified by the very small size of the other isotopic concentrations). The resulting change in k_{eff} is 0.0096 %Δk for the Pu-Al plates.

Now, the weight percent of ^{238}Pu, ^{241}Pu and ^{242}Pu in the assembly, before decaying ^{241}Pu, was less than 2%. The only isotope besides ^{239}Pu whose uncertainty would be expected to impact k_{eff} appreciably is ^{240}Pu. The

relative uncertainty in the ^{240}Pu weight percent is 0.037% for the Pu-Al plates. Modification of the ^{240}Pu weight percent led to a calculated effect on k_{eff} of 0.0010 %Δk for the Pu-Al plates. The combined uncertainty in k_{eff} due to the uncertainties in the original weight percents of the remaining three isotopes is assumed to be no larger than the ^{240}Pu values, i.e., it is taken to be ±0.0010 %Δk for the Pu-Al plates. In principal, the total uncertainty in the Pu isotopic fractions could be reduced using the constraint that the sum of these fractions was unity. Because this uncertainty component does not make a significant contribution to the total uncertainty in the system reactivity, further analysis appears unwarranted.

Much of the ^{241}Pu that was in the fuel plates when they were manufactured decayed by the time ZPR-6/10 was built. The Pu/Al plates were made in 1960. ZPR-6/10 loading 24 was made critical on September 30, 1981 and the half-life of ^{241}Pu is 14.29 years.[a] The numbers in the inventory database are normalized to January 1, 1977. The estimated uncertainty in the decay constant is 1%. Increasing the decay constant increases the ^{241}Am mass and decreases the ^{241}Pu mass on the date of the experiment. Increasing the decay constant by 1% changes k_{eff} by 0.0029 %Δk for ZPR-6/10 Loading 24.

Trace impurities in the plutonium fuel are known only to be small (approximately 0.2 wt.%) and are assumed to have a negligible effect on the total plutonium mass uncertainty. The quadrature sum of all the plutonium uncertainty effects, i.e., mass, weight percents and decay constant, is 0.0319 %Δk. This uncertainty is dominated by the plutonium mass uncertainty.

The uncertainty in the mass of aluminum from the Pu/Al fuel alloy was computed in the same way as the plutonium mass uncertainty. The computed aluminum mass uncertainty is 0.10%. Since changing the core region aluminum atom density by this amount changes k_{eff} by less than 0.0001 %Δk this uncertainty will not be carried forward.

The assumed 0.15% uncertainty in the mass of the graphite plates was calculated to have a 0.0201 %Δk effect.

The graphite plates are listed in the hot constants memo as being 100% C. These plates would have been nuclear grade graphite similar to CP-2 graphite. Table 2.1 shows the results of an analysis of CP-2 graphite performed by Evans Analytical Group for Idaho National Laboratory in 2012[b]. The worth of the impurities shown in Table 2.1 was calculated with the ZPR-6/10 as-built model. The computed worth of these impurities is 0.0090 ± 0.0060 %Δk. The uncertainty in the impurity content for the ZPR-6 graphite plates is assumed to be 50% of the values listed in Table 2.1. Consequently, the total uncertainty for the impurities in the graphite plates is the quadrature sum of the Monte Carlo statistical uncertainty and 0.0045 %Δk (0.0090/2) which is 0.0075 %Δk. The graphite impurities are not included in the as-built or benchmark models, so neglecting these impurities is treated as a bias in Section 3.5.

The graphite plates used in ZPR-3 were coated with a mixture of titanium oxide and Teflon. The graphite plates in the ZPR-6 inventory definitely were not coated[c].

The hot constants memo states that the graphite plates used in ZPR-6 contained 0.001 – 0.02 wt.% hydrogen. It is assumed that the average hydrogen content in these graphite plates was 100 ppm with a 100 ppm uncertainty which is treated as a bounding uncertainty with uniform probability distribution. The computed worth of the 100 ppm hydrogen uncertainty is 0.1091/√3 or 0.0630 %Δk. The hydrogen is not included in the as-built or benchmark models, so neglecting the hydrogen is treated as a bias in Section 3.5.

[a] E. M. Baum et al, "Nuclides and Isotopes – Chart of Nuclides," Seventeenth Edition, Revised 2009, Knolls Atomic Power Laboratory.
[b] Table 2.1 was provided by J. D. Bess of Idaho National Laboratory.
[c] J. A. Morman, Personal Communication, June 2015.

The quadrature sum of the uncertainties related mass, impurities and hydrogen content for the graphite plates is 0.0665 %Δk which is dominated by the hydrogen uncertainty.

Table 2.1. Measured Impurities in CP-2 Graphite.

Element	Concentration [ppm wt]	Element	Concentration [ppm wt]
Li	0.67	Pd	<0.05
Be	<0.05	Ag	<0.05
B	0.35	Cd	<0.05
C	Matrix	In	<0.05
N	-	Sn	<0.05
O	-	Sb	<0.05
F	<0.1	Te	<0.05
Na	<0.05	I	<0.01
Mg	0.06	Cs	<0.05
Al	2.2	Ba	<0.05
Si	70	La	<0.05
P	0.65	Ce	<0.05
S	45	Pr	<0.05
Cl	0.45	Nd	<0.05
K	<0.1	Sm	<0.01
Ca	160	Eu	<0.01
Sc	<0.01	Gd	<0.01
Ti	12	Tb	<0.01
V	120	Dy	<0.01
Cr	<0.5	Ho	<0.01
Mn	0.02	Er	<0.01
Fe	6.2	Tm	<0.01
Co	<0.01	Yb	<0.01
Ni	1.4	Lu	<0.01
Cu	0.15	Hf	<0.01
Zn	<0.05	Ta	<100
Ga	<0.01	W	<0.05
Ge	<0.05	Re	<0.01
As	<0.05	Os	<0.01
Se	<0.05	Ir	<0.01
Br	<0.1	Pt	<0.01
Rb	<0.05	Au	<0.1
Sr	1.2	Hg	<0.1
Y	<0.05	Tl	<0.05
Zr	0.34	Pb	<0.05
Nb	<0.05	Bi	<0.05
Mo	<0.05	Th	<0.05
Ru	<0.05	U	<0.05
Rh	<0.01		

The matrix tubes, drawers, Pu-Al clad and stainless steel plates used in ZPR-6/10 were obtained at different times from different vendors. Further, the stainless steel plates came from three distinct lots designated as SSTX, SS75 and SST in the ZPR records. These plate lots also were obtained at different times and probably from different vendors. Consequently, the matrix tubes, drawers, Pu-Al clad, SSTX plates, SS75 plates and SST plates are considered to be independent and uncorrelated.

It is estimated that the mass of the matrix tubes is uncertain by 2%[a], and the masses of all the other iron and stainless steel components are uncertain by 0.15%. The estimated weight percent uncertainty data for the iron and stainless steel are presented in Table 2.2. A representative value of the weight percent is shown in parentheses. The uncertainty for each of the major elements was taken (conservatively) to be 0.2 wt.%. The uncertainty for Mn in the stainless steel was taken to be 0.15 wt.% (or 10% of nominal value) based on the variation of batch assays given in the hot constants memos. Given that the various batches of steel plates were intermixed over years of operation of the ZPR facilities, it is no longer possible to better quantify the uncertainty derived from using the nominal values stated in the hot constants memos. The uncertainties for the remaining minor elements were assumed to be one half of the last significant figure provided in the hot constants memos, due to round-off error. The uncertainty for the sum of trace elements was assumed to be 10% of the typical wt.%.

Table 2.2. Iron and Steel Weight Percent Uncertainty Data.

Element	(Nominal Value) ± Uncertainty , wt.%	
	Iron Plates	Stainless Steel
Fe	(99.31) ± 0.2	(70) ± 0.2
Cr		(18) ± 0.2
Ni		(9.5) ± 0.2
Mn	(0.50) ± 0.005	(1.5) ± 0.15
Mo		(0.3) ± 0.005
Si	(0.02) ± 0.005	(0.3) ± 0.005
C	(0.10) ± 0.005	(0.05) ± 0.005
Cu+S+P	(0.04) ± 0.004	(0.35) ± 0.035

The k_{eff} uncertainty contributions due to the weight percent uncertainty for the elements comprising the iron plates and stainless steel plates were computed by perturbing the reference DIF3D-VARIANT model using the data in Table 2.2. The results by element and component category for the stainless steel and iron plates are shown in Table 2.3. The effects of uncertainties in Si, C, Cu, S and P were neglected because a) their uncertainties are small compared to the uncertainties for Fe, Cr, Ni and Mn and b) Si, C, Cu, S and P are not significant absorbers in the ZPR-6/10 spectrum. The total mass of each material was conserved when the composition was perturbed. On an element basis, the contributions from the Mn wt.% uncertainty dominate, which is most unusual. It is hypothesized that the sensitivity is due to low-energy Mn cross section resonances coupled with an unusually large flux at those energies (see Appendix C).

[a] The 2% mass uncertainty for the matrix tubes is a value developed by R. Schaefer and R. D. McKnight, former ZPPR and ZPR staff analysts, to provide a reasonable upper limit for the uncertainty in the mass of the matrix tubes in ZPR-3, ZPR-6, ZPR-9 and ZPPR. The number of matrix tubes ranges from 1922 for ZPR-3 to ~11858 for ZPPR, so it seems plausible that normal manufacturing variations would produce an uncertainty larger than the 0.15% uncertainty for the weights of standard plates. The reactivity effect of the matrix tube mass uncertainty is not a dominant uncertainty in ZPR and ZPPR assemblies, and there is no information available to justify a different value.

Table 2.3. Contribution from Iron and Steel Weight% Uncertainty to k_{eff} Uncertainty (%Δk).

Component	Matrix	SSTX Plates	SS75 Plates	SST Plates	Drawers	Pu-Al Clad	Iron Plates
Mass	0.0155	0.0033	0.0064	0.0021	0.0005	0.0001	<0.0001
Fe	0.0012	0.0034	0.0058	0.0019	0.0006	0.0001	
Cr	0.0011	0.0034	0.0059	0.0019	0.0007	0.0001	<0.0001
Ni	0.0015	0.0032	0.0093	0.0030	0.0008	0.0001	
Mn	0.0154	0.0630	0.0111	0.0025	0.0086	0.0028	
Quadrature Sum	0.0220	0.0634	0.0179	0.0052	0.0087	0.0028	<0.0001

The quadrature sum all the steel and iron uncertainty effects, weight percent and mass, is ±0.0702 %Δk.

A very small bias and uncertainty due to the presence of humidity in the air was derived for an earlier ZPR assembly. This was done by comparing calculations with the assembly gaps filled by dry air and by saturated air. The calculated effect, 0.0001% Δk, is assumed to apply to this assembly and will be included simply as an uncertainty.

2.4 Combined Uncertainties and Final Excess Reactivity

All of the uncertainties discussed in the previous sections are summarized in Table 2.4. None of the uncertainties in the measurement technique category is important. Only the matrix tube pitch uncertainty is of any consequence in the geometry category. Its effect is comparable to that of the plutonium composition uncertainty but both are dominated by the effect of the graphite moisture and SSTX stainless steel plate composition uncertainties. The SSTX plate effect comes predominately from the sensitivity to the Mn in the stainless steel. This most unusual outcome appears to be the consequence of low-energy Mn cross section resonances, coupled with the unusual core-region spectrum in ZPR-6/10 (see Appendix C).

The measured excess reactivity of 78.5 Ih converts to 0.0688 %Δk. The estimated total uncertainty in Table 2.4, 0.1089 %Δk, is larger than this, yet there is no doubt that the assembly was slightly supercritical. The uncertainty estimate is believed to be conservative but reasonable. Treating the uncertainty as if it were 1σ of a normal distribution should be acceptable for the purposes of the benchmark model. As discussed in Section 2.2, this uncertainty covers the effects of simplifying adjustments to the experiment, such as removal of the matrix interface gap. The adjustments are addressed further in Section 3.5.

Table 2.4. Summary of the Uncertainties in the Experimental k_{eff} for ZPR-6/10.

Source of Uncertainty	Uncertainty in Excess Reactivity (% Δk)
Measurement Technique	
Excess reactivity (including temperature uncertainty)	0.0020
Reproducibility	0.0023
Inhour to Δk conversion	0.0034
Subtotal	**0.0046**
Geometry	
Matrix interface gap	0.0073
Nominal plate dimensions	0.0058
PSR blade position	0.0030
Matrix tube pitch	0.0370
Room return	0.0026
Subtotal	**0.0384**
Composition	
Plutonium mass	0.0302
^{239}Pu concentration	0.0096
^{240}Pu concentration	0.0010
Other Pu isotopes	0.0010
^{241}Pu decay	0.0029
Graphite mass	0.0201
Graphite impurities	0.0075
Graphite moisture	0.0630
Matrix tubes	0.0220
SSTX plates	0.0634
SS75 plates	0.0179
SST plates	0.0052
Drawers	0.0087
Pu-Al clad	0.0028
Iron	0.0001
Humidity	0.0001
Subtotal	**0.1018**
Total	**0.1089**

ZPR-6/10 has been determined to be an acceptable criticality-safety benchmark experiment.

3.0 BENCHMARK SPECIFICATIONS

3.1 Description of Model

Even the most casual perusal of Section 1 makes it clear that ZPR-6/10 Loading 24 is too complicated to be a practical criticality-safety benchmark model without a great deal of simplification. Fortunately, it is possible to eliminate virtually all of the complexity and to obtain a simple benchmark model without losing any of the essential physics. Furthermore, this can be done without compromising the high accuracy of the experiment.

This was accomplished by computing the transformation from the detailed as-built experiment model to the simple benchmark model using the a continuous-energy Monte Carlo code. Note that the term "transformation" will be used repeatedly through Section 3 and will, in all cases, refer to both the simplification of the model from the as-built platewise heterogeneous experiment model to the homogeneous cylindrical benchmark model, and also the correction of k_{eff} to account for these simplifications. Continuous energy Monte Carlo eigenvalue calculations were made for the as-built model and for the benchmark model. The k_{eff} correction is simply the difference in k_{eff} between the two models.

The modeling of all the experimental detail was made tractable by the development of the BLDVIM computer code[a] to generate the VIM input file for the as-built model. BLDVIM reads an electronic database containing a description of the ZPPR plate and drawer inventory, the assembly drawer masters, and the matrix loading maps. The code and database were rewritten for UNIX-based workstations, at which time the values of Avogadro's number and the atomic masses were made to conform to the values recommended by the ICSBEP.

VIM input requires that an edit region number be assigned to each geometric region. Each geometric region associated with the ZPR-6/10 core (each plate, air gap, drawer segment, etc.) was assigned edit region number 1. Similarly, each geometric region of the axial reflector was assigned edit region number 2, and so on. Of course, the composition (atom densities) associated with each geometric region of the as-built model must also be assigned. These assignments were made with the aid of the BLDVIM code, reducing the actual hand-generated input from thousands of numbers to just a few. When the resulting as-built model was processed by the VIM code, the total volume and the volume-averaged atom densities for each edit region were edited. These edits were used to derive the benchmark model as follows.

The key features retained in the benchmark model are the region-averaged compositions, region volumes, and the global geometry. The geometry is depicted in Figure 3-1. The radial dimensions of the benchmark model were determined by the total cross-sectional area of the matrix positions included in each region, i.e., radii of cylindrical boundaries conserve cross-sectional areas of the corresponding regions in the as-built model. Axial dimensions of each region were then set to conserve the edit-region volume. Finally, the edit-region atom densities were assigned to the corresponding benchmark model regions.

[a] R. W. Schaefer, R. D. McKnight and P. J. Collins, "Lessons Learned from Applying VIM to Fast Reactor Critical Experiments," *Proceedings of the Nuclear Criticality Technology Safety Workshop*, San Diego, CA, pp. 129-136, LA-13439-C (1995).

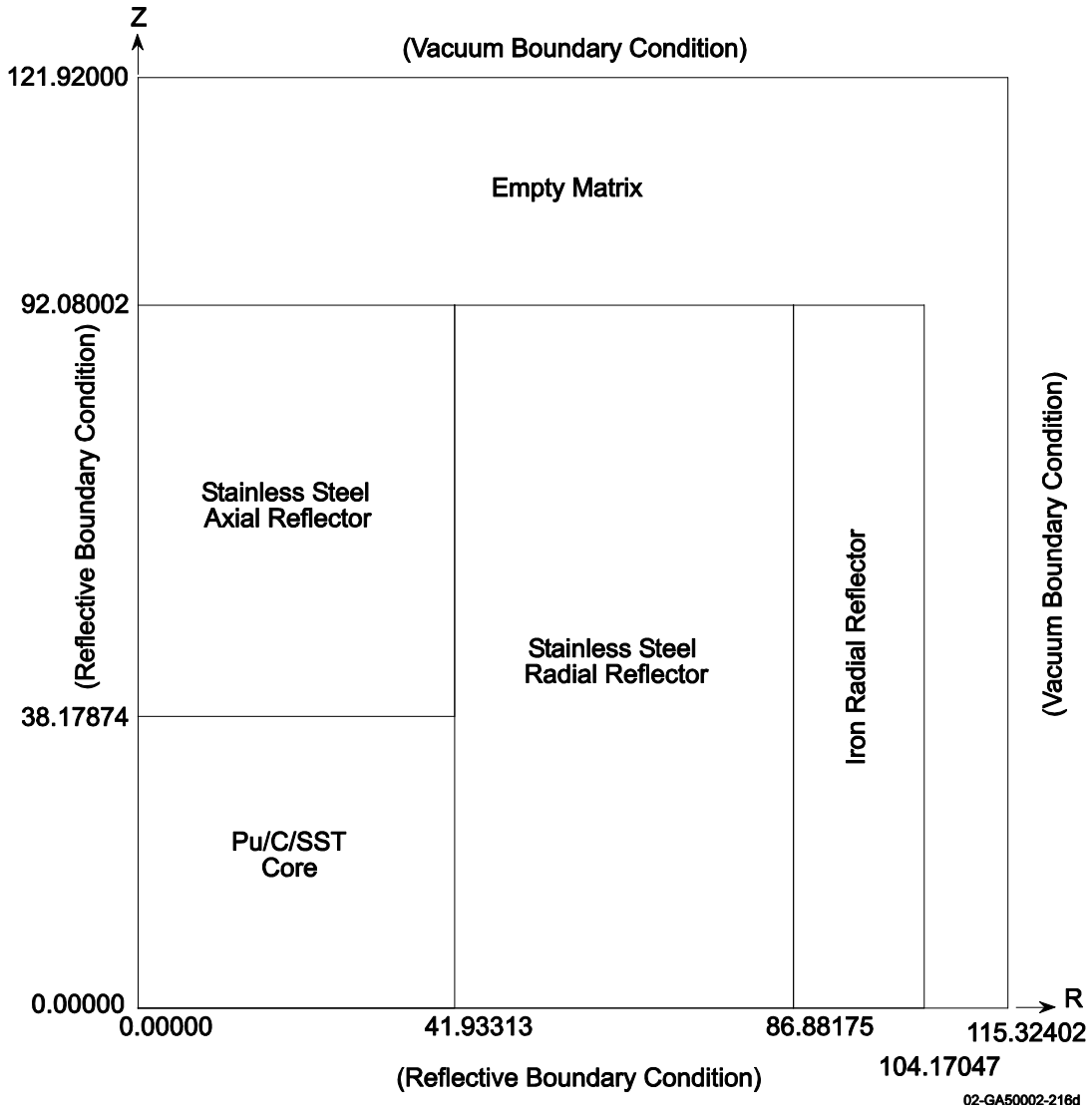

Figure 3-1. Benchmark-Model Geometry for ZPR-6/10.

Obvious simplifications made were the smoothing of jagged boundaries in the XY plane into circular boundaries and the elimination of some of the empty matrix. The simplification that yielded by far the greatest elimination of detail was the smearing of plates, drawers, and matrix tubes into cylindrical regions. The plate heterogeneity effects, which would require much effort to capture accurately in effective homogenized cross sections in a deterministic modeling approach, are included in the Monte Carlo-calculated Δk of the transformation.

Several minor simplifications of the experiment were made in developing the as-built model and these implicitly apply to the benchmark model as well. The small gap between the matrix halves was neglected. A matrix pitch slightly different from the best-estimate pitch for this assembly was used. The poison control rods were omitted because they were in the fully withdrawn position, where their worth was negligible.

The outer portion of the empty matrix and its support structures were judged to have a negligible room return effect and were omitted. Finally, humid air was replaced by void in all the air gaps. All of these biases and their associated uncertainties were quantified in Section 2 and their impact on k_{eff} is summarized in Section 3.5.

3.2 Dimensions

The benchmark model consists of only five regions, as shown in Figure 3-1. The central region is a cylindrical core with a radius of 41.93313 cm and a half-height of 38.17874 cm. A stainless steel axial reflector with the same radius extends axially to 92.08002 cm. A stainless steel radial reflector goes to this height from the axial midplane and extends radially from the core boundary to 86.88175 cm. An iron radial reflector surrounds the stainless steel one, has the same axial extent and extends radially to 104.17047 cm. A portion of the empty matrix surrounding the reflectors forms the outermost region. Radially it extends to 115.32402 cm, representing the empty corners of the 37x37 section of the matrix that is shown in Tables 1 and 2. Axially it extends to 121.92 cm, which is the end of the matrix tubes.

3.3 Material Data

Tables 3.1 and 3.2 show the region-dependent composition data for the benchmark model. The masses of ^{241}Pu and ^{241}Am correspond to September 30, 1981. These atom densities came directly from the edit-region output from the VIM code calculation of the as-built model as described in Section 3.1.

Table 3.1. Core Region Composition (atoms/barn-cm).

Nuclide	Core
^{238}Pu	1.69380E-09
^{239}Pu	1.06299E-03
^{240}Pu	5.03037E-05
^{241}Pu(a)	1.70034E-06
^{242}Pu	1.15592E-07
^{241}Am(a)	2.98613E-06
Cr	9.84199E-03
Al	1.11659E-04
Mn	8.05254E-04
Co	3.71924E-06
Ni	4.08528E-03
C	2.58213E-02
Cu	1.01231E-04
Fe	3.52607E-02
Mo	7.42792E-05
Si	2.79577E-04

(a) Masses of ^{241}Pu and ^{241}Am correspond to September 30, 1981.

Table 3.2. Reflector and Matrix Compositions (atoms/barn-cm).

Nuclide	Axial Stainless Steel Reflector	Radial Stainless Steel Reflector	Iron Radial Reflector	Empty Matrix
Cr	1.57277E-02	1.56286E-02	1.82758E-03	1.18727E-03
Mn	1.56081E-03	1.42057E-03	5.50350E-04	1.05699E-04
Co	3.73582E-06	3.77932E-06	3.77222E-06	0.00000E-00
Ni	6.94657E-03	6.78410E-03	7.61435E-04	4.79539E-04
C	2.35948E-04	2.37106E-04	4.27315E-04	1.87078E-05
Cu	2.98115E-05	5.04052E-05	2.90457E-05	1.71849E-05
Fe	5.55221E-02	5.51964E-02	7.66532E-02	4.27243E-03
Mo	1.52120E-05	4.64023E-05	1.46235E-05	8.23697E-06
Si	9.45490E-04	8.63360E-04	1.45148E-04	6.81747E-05

3.4 Temperature Data

The experimenters reported the excess reactivity corresponding to a temperature of 25ºC, which is approximately room temperature. That is the temperature used for the benchmark model. The measured temperature coefficient, approximately –0.004 %Δk/ºC, can be used if a temperature adjustment is desired.

3.5 Experimental and Benchmark Model k_{eff}

The transformation Δk (bias) from the as-built configuration to the benchmark model was calculated using a continuous-energy Monte Carlo code with ENDF/B-VII.1 data. The results are shown in Table 3.3. The uncertainties shown are just the statistical standard deviations from the Monte Carlo calculations.

Table 3.3. Eigenvalues for Transformation From As-Built Model to RZ Benchmark Model.

As-built Model k_{eff}	RZ Benchmark Model k_{eff}	Transformation Δk (Bias)
1.0276 ± 0.0001	1.0148 ± 0.0001	-0.0128 ± 0.0002

An estimate of the total uncertainty in the transformation Δk from the as-built, platewise heterogeneous critical-assembly model to the homogeneous cylindrical model is needed. Since there are no significant geometric approximations in the as-built model and there are no cross section processing approximations associated with either model, the only sources of uncertainty added to the original experimental uncertainty come from the Monte Carlo statistical precision and the sensitivity of the calculated Δk values to uncertainties in the basic cross section data. The major cross section uncertainties in the assembly arise from fission production and absorption in ^{239}Pu. Uncertainties in the k_{eff} of fast reactor critical assemblies due to calculations with ENDF/B-V data have been quantified.[a] In a set of about a dozen assemblies, the k_{eff} uncertainty ranges from 1.1% to 2.0%. The conservative assumption is made that the high end of this range,

[a] Table IV in: D. N. Olsen, P. J. Collins and S. G. Carpenter, "Experiments of IFR Fuel Criticality in ZPPR-21," *ICNC '91 International Conference on Criticality Safety*, Oxford, UK, September 9-13, 1991.

2.0%, (which happens to be for the plutonium-fueled assembly ZPPR Assembly 21A) applies to the k_{eff} of ZPR-6/10.

Because there is a strong correlation between the two calculations, the transformation Δk has a much smaller uncertainty than the uncertainty in either k_{eff}. The two calculations for the transformation Δk are based on the same code and on the same cross sections, with similar sensitivities of k_{eff} to the cross sections, and are thus highly correlated. The ensuing uncertainty in the transformation Δk is therefore assumed smaller by an order of magnitude, or ±0.20% Δk. Adding in quadrature the uncertainties due to use of ENDF/B cross sections and the uncertainty from statistics on the difference of the two Monte Carlo calculations yields a total uncertainty in the transformation Δk of 0.20% Δk.

This uncertainty estimate is believed to be conservative but still sufficiently small for criticality-safety benchmark purposes. The actual correlations are likely higher than the values assumed in deriving the estimated uncertainty. The transformation Δk is discussed further in Appendix B.

Several small adjustments to the measured k_{eff} are needed to account for differences between the actual experiment conditions and the as-built model. The matrix-interface gap, estimated to be 0.0635 cm, was not included in the as-built model. Removal of this gap increases k_{eff} by 0.0146 %Δk, based on the gap worth measurement data. The models are based on a square matrix pitch of 2.175 inches, which is the pitch that has been used in analysis and reporting of ZPR assemblies for decades. Adjusting from the effective square pitch measured for ZPR-6/10, 2.177 inches, to 2.175 inches increases k_{eff} by 0.0748 %Δk. The poison control rods (PSRs), which were withdrawn deep in the axial reflector, were omitted from the models. Their reactivity effect at the withdrawn position is so small, < 0.0003 %Δk, that this effect was treated as an uncertainty rather than an adjustment. The models end a short distance into the empty matrix beyond the plate-loaded drawers. Omission of the remaining empty matrix and the massive supporting structures had a negligible effect on k_{eff}. As noted in Section 2.3, the effect of omitting humid air from the models (replaced by void) is so small, 0.0001 %Δk, that this effect was treated as an uncertainty rather than an adjustment.

Two additional adjustments are needed for the graphite plates. Neglecting the impurities in the graphite plates listed in Table 2.1 increases k_{eff} by 0.0090 %Δk. Neglecting the hydrogen in the graphite reduces k_{eff} by 0.1091 %Δk.

The uncertainty contributions from all of these differences were included in the uncertainty evaluations in Section 2.

The data for the experimental and benchmark-model k_{eff} values are summarized in Table 3.4. The data in the table are in units of k_{eff}. The measured k_{eff} reflects the excess reactivity from Section 2.1. The adjustments leading to the adjusted experimental k_{eff} were just discussed. The uncertainty in the adjusted value is the total uncertainty from Table 2.4 in Section 2.4. Applying the Monte Carlo transformation to the adjusted experimental k_{eff} yields the benchmark model k_{eff} shown on the last line.

Table 3.4. Experimental and Benchmark-Model Eigenvalues.[a]

Measured k_{eff}	1.00069
Remove matrix interface gap	0.00015
Reduce matrix pitch	0.00074
Eliminate room return	Negligible
Neglect graphite impurities	0.00009
Neglect H in graphite	-0.00109
Adjusted experimental k_{eff}	1.0006 ± 0.0011
Monte Carlo transformation of model	-0.0128 ± 0.0020
Benchmark model k_{eff}	0.9878 ± 0.0023

(a) Each uncertainty estimate is one standard deviation.

4.0 RESULTS OF SAMPLE CALCULATIONS

Results of sample calculations of the benchmark model of Case 1, ZPR-6/10 Loading 24, are given in Table 4.1. More details of the calculations, including input listings, are given in Appendix A. Additional results are given in Appendix B. Appendix C displays the calculated neutron spectrum and presents a detailed neutron balance. The benchmark model k_{eff} for Case 1 is 0.9878 ± 0.0023.

Table 4.1. Sample Calculation Results for Case 1, ZPR-6/10 Loading 24.

Code	Cross Sections	Calculation		C/E - 1	
		k_{eff}	σ	C/E-1, %	σ, %
KENO V.a	238-Group ENDF/B-V	1.0269	0.0009	3.96	0.26
KENO V.a	27-Group ENDF/B-IV	1.0262	0.0009	3.89	0.26
MCNP-4B	Cont. Energy ENDF/B-V	1.0038	0.0010	1.62	0.26
MCNP-4C	Cont. Energy ENDF/B-V	0.9945	0.0005	0.68	0.24
MCNP-4C	Cont- Energy ENDF/B-VI	1.0245	0.0005	3.72	0.25
VIM	Cont. Energy ENDF/B-V	0.9862	0.0005	-0.16	0.24
VIM	Cont. Energy ENDF/B-VI	1.0222	0.0006	3.48	0.25
MONK-8B[(a)]	8220-Group UKNDL	1.0444	0.0009	5.73	0.26
MONK-8B[(a)]	13193-Group JEF-2.2	1.0115	0.0009	2.40	0.26
MONK-8B[(a)]	13193-Group ENDF/B-VI	1.0324	0.0009	4.52	0.26
MCNP6	Cont. Energy ENDF/B-VII.1	1.0148	0.0001	2.73	0.24

(a) Results supplied by M. A. Smith (ANL)

The MCNP6 result with ENDF/B-VII.1 data in the bottom row of Table 4.1 was computed in 2016 for Revision 1. All of the other results in Table 4.1 were computed in 2002 for Revision 0. The 2002 results are retained here partly for historical reasons and partly because they clearly illustrate the effect of the transition from ENDF/B-V.2 to ENDF/B-VI and ENDF/B-VII on calculations for this assembly.

Only two k_{eff} results are within 1% of the experimental benchmark k_{eff}, 0.9878. They are the results computed using ENDF/B-V cross section data with a continuous-energy Monte Carlo method that includes a rigorous treatment of unresolved resonances (VIM and MCNP-4C codes). The importance of the resonance treatment stems from the high flux level in the resonance range, which is shown in Appendix C. The importance for this benchmark of a rigorous treatment of unresolved resonances is illustrated by the nearly 1% higher k_{eff} obtained when MCNP Version 4B, which has an approximate treatment, is used instead of Version 4C. Clearly, the k_{eff} of this benchmark is extraordinarily sensitive to details in the processing of resonance cross sections.

Results using alternative iron cross sections in MCNP-4C are presented in Appendix B.3, which also show a strong sensitivity. It is apparent that ZPR-6/10 would serve as a very useful benchmark for cross section data testing.

Given this behavior, a strong sensitivity to basic cross section data would be expected and, indeed, is evident from Table 4.1. The VIM results using ENDF/B-VI data is ~3.6% higher than the result using ENDF/B-V data, and the VIM result using ENDF/B-VII.0 data is ~3.7% higher than the result using ENDF/B-V data. The MCNP results using ENDF/B-VI data and ENDF/B-VII data do not differ significantly from the corresponding VIM results. Also, the large reactivity increase with ENDF/B-VI and –VII does not depend on which model of ZPR-6/10 is used; the same difference between ENDF/B-V and later releases is observed in calculations with the detailed as-built model and with the RZ benchmark model. For this assembly, Versions VI, VII.0 and VII.1 of ENDF/B yield a much larger bias relative to the benchmark k_{eff} than ENDF/B-V.

The source of the large change in the calculated values between ENDF/B-V and later ENDF releases was investigated by systematically replacing ENDF/B-V isotopes or elements in the VIM as-built model with the corresponding ENDF/B-VI and ENDF/B-VII.0 isotopes or elements. In most cases, the effects of replacing ENDF/B-V elements and isotopes with ENDF/B-VI and –VII versions were small and largely cancelled each other out. There were, however, three important exceptions. Replacing ENDF/B-V ^{239}Pu by ^{239}Pu from later releases raised k_{eff} by 1%Δk, and replacing ENDF/B-V ^{55}Mn by ^{55}Mn from ENDF/B-VI and ENDF/B-VII.0 raised k_{eff} by 0.9%Δk. The most important change, however, relates to Cr. Replacing the elemental ENDF/B-V Cr by the isotopic Cr in ENDF/B-VI or –VII increased k_{eff} by 1.8%Δk. Since ENDF/B-V Cr was elemental, it is not possible to determine exactly which Cr isotopes are responsible for the 1.8%Δk change. The sum of the reactivity changes between ENDF/B-V and later ENDF/B releases due to ^{239}Pu, ^{55}Mn and Cr is 3.7%Δk which entirely accounts for the observed difference in k_{eff} between ENDF/B-V and later ENDF/B releases.

5.0 REFERENCES

The ZPR-6 and ZPR-9 facilities were permanently shut down shortly after the last experiment was conducted on ZPR-6 Assembly 10. At that time all of the experimenters were given unrelated assignments. Consequently, only one open-literature publication was produced for experiments performed on this assembly.

1. E. F. Bennett, "An Experimental Method for Reactor-Noise Measurements of Effective Beta," Argonne National Laboratory Report ANL-81-72 (1981).

APPENDIX A: TYPICAL INPUT LISTINGS

There is only one case, Case 1, for this evaluation. ASCII text files for the MCNP and VIM input files for Case 1 are provided in two subfolders which are located in the input folder of the directory of this evaluation. The individual input files are identified as **case_01_xx_yy** where "xx" is either "ab" for a detailed as-built model or "rz" for the RZ benchmark model. The "yy" qualifier is "52" for a model with ENDF/B-V.2 nuclides specified, "70" for a model with ENDF/B-VII.0 nuclides specified or "71" for a model with ENDF/B-VII.1 nuclides specified.

A.1 KENO Input Listings

A sample input for the SCALE/KENO V.a 238-group calculation with ENDF/B-V data is shown below. The input for the SCALE/KENO V.a 27 group calculation with ENDF/B-IV data is the same except for the third line, where the cross section set is specified. The KENO calculations were run with 110 generations with 5000 histories per generation, skipping the first 10 generations, for a total of 500,000 active histories. Examination of the output confirmed that 10 generations is sufficient to establish the asymptotic fission source distribution.

```
KENO 238-Group Input Listing, Table 4.1.

=csas25    parm=size=200000
zpr6-10.L24 Plutonium-Graphite-Stainless Steel core with steel reflectors
238gr
infhommedium
PU-240              1  0.0  5.03034E-05  298  end
PU-241              1  0.0  1.70033E-06  298  end
PU-239              1  0.0  1.06298E-03  298  end
PU-238              1  0.0  1.69379E-09  298  end
PU-242              1  0.0  1.15591E-07  298  end
AM-241              1  0.0  2.98612E-06  298  end
CR                  1  0.0  9.84196E-03  298  end
NI                  1  0.0  4.08528E-03  298  end
FE                  1  0.0  3.52607E-02  298  end
AL                  1  0.0  1.11659E-04  298  end
C                   1  0.0  2.58213E-02  298  end
MO                  1  0.0  7.42790E-05  298  end
MN                  1  0.0  8.05253E-04  298  end
CU                  1  0.0  1.01231E-04  298  end
SI                  1  0.0  2.79577E-04  298  end
CO                  1  0.0  3.71922E-06  298  end
CR                  2  0.0  1.57277E-02  298  end
NI                  2  0.0  6.94658E-03  298  end
FE                  2  0.0  5.55223E-02  298  end
C                   2  0.0  2.35876E-04  298  end
MO                  2  0.0  1.52118E-05  298  end
MN                  2  0.0  1.56081E-03  298  end
CU                  2  0.0  2.98112E-05  298  end
SI                  2  0.0  9.45493E-04  298  end
CO                  2  0.0  3.73583E-06  298  end
CR                  3  0.0  1.56286E-02  298  end
NI                  3  0.0  6.78410E-03  298  end
FE                  3  0.0  5.51964E-02  298  end
C                   3  0.0  2.37106E-04  298  end
MO                  3  0.0  4.64023E-05  298  end
MN                  3  0.0  1.42057E-03  298  end
CU                  3  0.0  5.04052E-05  298  end
SI                  3  0.0  8.63360E-04  298  end
CO                  3  0.0  3.77932E-06  298  end
CR                  4  0.0  1.82758E-03  298  end
NI                  4  0.0  7.61435E-04  298  end
FE                  4  0.0  7.66532E-02  298  end
C                   4  0.0  4.27315E-04  298  end
MO                  4  0.0  1.46235E-05  298  end
MN                  4  0.0  5.50350E-04  298  end
```

```
CU                 4  0.0  2.90457E-05  298  end
SI                 4  0.0  1.45148E-04  298  end
CO                 4  0.0  3.77222E-06  298  end
CR                 5  0.0  1.18727E-03  298  end
NI                 5  0.0  4.79539E-04  298  end
FE                 5  0.0  4.27243E-03  298  end
C                  5  0.0  1.87078E-05  298  end
MO                 5  0.0  8.23697E-06  298  end
MN                 5  0.0  1.05699E-04  298  end
CU                 5  0.0  1.71849E-05  298  end
SI                 5  0.0  6.81747E-05  298  end
end comp
zpr6-10.L24 Plutonium-Graphite-Stainless Steel core with steel reflectors
read param  tme=199.0 gen=110 npg=5000 nsk=10 run=yes tba=3.0
end param
read geom
unit 1
cylinder  1  1    41.93313    38.17874    -38.17874
cylinder  2  1    41.933131   92.08002    -92.08002
cylinder  3  1    86.88175    92.080021   -92.080021
cylinder  4  1   104.17047    92.080022   -92.080022
cylinder  5  1   115.32402   121.92000   -121.92000
end geom
end data
end
```

A.2 MCNP Input Listings

A sample MCNP input is listed below. It invokes continuous energy ENDF/B-V cross sections for all nuclides by using the suffix 50c with the nuclide ID. This input applies to both the Version 4B and Version 4C calculations. The input for the calculations with continuous energy ENDF/B-VI cross sections is the same except that the nuclide ID suffix is 60c and elements are replaced by their naturally occurring isotopes. The Version 4C calculations used 25000 neutron histories per generation and 200 active generations, after skipping 40. It would have been more computationally efficient to skip fewer generations, since the asymptotic fission source distribution was established by about the tenth generation. The same values were used for the Version 4B calculation except there were only 2500 neutron histories per generation.

```
MCNP ENDF/B-V Input Listing, Table 4.1.

PU-MET-INTER-002 - ZPR-6/10 L024 - RZ Benchmark Model - V5 XS
c
c     Version 5 XS - MCNP5
c
1     1  7.750309e-2  -1   5  -6  imp:n=1 $ core
2     2  8.098731e-2   (-1 6 -8):(-1 -5 7)  imp:n=1 $ ss ax refl
3     4  8.023073e-2   1  -2  7 -8  imp:n=1 $ ss radial refl
4     5  8.041246e-2   2  -3  7 -8  imp:n=1 $ fe radial refl
5     3  6.157238e-3   (3 -4 9 -10):(-3 8 -10):
                       (-3 -7 9)  imp:n=1 $ empty matrix
6     0                (4:-9:10)  imp:n=0 $ external void

1     cz     41.93313
2     cz     86.88175
3     cz    104.17047
4     cz    115.32402
5     pz    -38.17874
6     pz     38.17874
7     pz    -92.08008
8     pz     92.08008
9     pz   -121.92000
10    pz    121.92000

mode  n
kcode  20000  1.0  100  600
sdef   erg=d1 rad=d2 ext=d3 pos 0 0 0.0 axs 0 0 1
sp1    -2
si2    0.0  41.93
si3    -38.0  38.0
m001     94240.50c   5.03037E-05     94241.50c   1.70034E-06 $ Core
         94239.50c   1.06299E-03     94238.50c   1.69380E-09
         94242.50c   1.15592E-07     95241.50c   2.98613E-06
         24000.50c   9.84199E-03     28000.50c   4.08528E-03
         26000.50c   3.52607E-02     13027.50c   1.11659E-04
          6000.50c   2.58213E-02     42000.50c   7.42792E-05
         25055.50c   8.05254E-04     29000.50c   1.01231E-04
         14000.50c   2.79577E-04     27059.50c   3.71924E-06
m002     24000.50c   1.57277E-02     28000.50c   6.94657E-03 $ Axial refl
         26000.50c   5.55221E-02      6000.50c   2.35948E-04
         42000.50c   1.52120E-05     25055.50c   1.56081E-03
         29000.50c   2.98115E-05     14000.50c   9.45490E-04
         27059.50c   3.73582E-06
m003     24000.50c   1.18727E-03     28000.50c   4.79539E-04 $ Matrix
         26000.50c   4.27243E-03      6000.50c   1.87078E-05
         42000.50c   8.23697E-06     25055.50c   1.05699E-04
         29000.50c   1.71849E-05     14000.50c   6.81747E-05
m004     24000.50c   1.56286E-02     28000.50c   6.78410E-03 $ SS rad refl
         26000.50c   5.51964E-02     13027.50c   1.00000E-20
          6000.50c   2.37106E-04     42000.50c   4.64023E-05
         25055.50c   1.42057E-03     29000.50c   5.04052E-05
         14000.50c   8.63360E-04     27059.50c   3.77932E-06
m005     24000.50c   1.82758E-03     28000.50c   7.61435E-04 $ Fe rad refl
         26000.50c   7.66532E-02      6000.50c   4.27315E-04
         42000.50c   1.46235E-05     25055.50c   5.50350E-04
```

```
         29000.50c   2.90457E-05     14000.50c   1.45148E-04
         27059.50c   3.77222E-06
totnu
phys:n  20.0  0.0
prdmp      J   40
ctme     9000.0
```

A.3 TWODANT Input Listings

A sample TWODANT input listings is not provided here because none of the TWODANT calculations utilized a standard multigroup cross section set. However, most of the sensitivity results presented in Section 2 were computed using TWODANT with a 20 group cross section set that was generated from ENDF/B-V data using the MC^2-2 code. Some TWODANT results and a sample TWODANT input listing are presented in Appendix B.

A.4 MONK8B Input Listings

A sample MONK input is shown below. MONK8B results were obtained using the UKNDL library (with 8220 groups), using the JEF2.2 library (with 13193 groups), and using the ENDF/B-VI library (with 13193 groups). Each calculation used 1000 superhistories per stage and was run to achieve a precision of 0.0005.

```
MONK JEF Input Listing, Table 4.1.

* Summary of experiment
* ----------------------
* Fissile Material:         Plutonium (PuAl)
* Geometry:                 Plate Lattice
* Neutron Poison:           None
* Reflectors:               Stainless Steel and Iron
* Reference:                R. W. Schaefer, R. M. Lell, R. D. McKnight and M A. Smith
*                           ZPR Assembly 10 Loading 24
*                           A Pu Cylinder Reflected
*                           by Stainless Steel and Iron
* Code Package:             MONK8B

* Notes
* -----
* The measured experiment temperature was 25C.
* However, note that the MONK data temperature is 20C.
*
************************************************************

BEGIN MATERIAL SPECIFICATION

NMATERIALS 5

* material  1 - core
* material  2 - axial reflector
* material  3 - radial reflector
* material  4 - iron reflector
* material  5 - empty matrix

ATOMS
MATERIAL  1 DENSITY 0.0
PU240 PROP  5.03034E-05
PU241 PROP  1.70033E-06
PU239 PROP  1.06298E-03
PU238 PROP  1.69379E-09
PU242 PROP  1.15591E-07
AM241 PROP  2.98612E-06
CR    PROP  9.84196E-03
NI    PROP  4.08528E-03
FE    PROP  3.52607E-02
AL    PROP  1.11659E-04
C     PROP  2.58213E-02
MO    PROP  7.42790E-05
MN    PROP  8.05253E-04
CU    PROP  1.01231E-04
SI    PROP  2.79577E-04
CO    PROP  3.71922E-06
ATOMS
MATERIAL  2 DENSITY 0.0
PU240 PROP  0.00000E+00
PU241 PROP  0.00000E+00
PU239 PROP  0.00000E+00
PU238 PROP  0.00000E+00
PU242 PROP  0.00000E+00
AM241 PROP  0.00000E+00
CR    PROP  1.57277E-02
NI    PROP  6.94658E-03
FE    PROP  5.55223E-02
AL    PROP  0.00000E+00
C     PROP  2.35876E-04
```

```
MO    PROP  1.52118E-05
MN    PROP  1.56081E-03
CU    PROP  2.98112E-05
SI    PROP  9.45493E-04
CO    PROP  3.73583E-06
ATOMS
MATERIAL  3 DENSITY 0.0
PU240 PROP  0.00000E+00
PU241 PROP  0.00000E+00
PU239 PROP  0.00000E+00
PU238 PROP  0.00000E+00
PU242 PROP  0.00000E+00
AM241 PROP  0.00000E+00
CR    PROP  1.56286E-02
NI    PROP  6.78410E-03
FE    PROP  5.51964E-02
AL    PROP  0.00000E+00
C     PROP  2.37106E-04
MO    PROP  4.64023E-05
MN    PROP  1.42057E-03
CU    PROP  5.04052E-05
SI    PROP  8.63360E-04
CO    PROP  3.77932E-06
ATOMS
MATERIAL  4 DENSITY 0.0
PU240 PROP  0.00000E+00
PU241 PROP  0.00000E+00
PU239 PROP  0.00000E+00
PU238 PROP  0.00000E+00
PU242 PROP  0.00000E+00
AM241 PROP  0.00000E+00
CR    PROP  1.82758E-03
NI    PROP  7.61435E-04
FE    PROP  7.66532E-02
AL    PROP  0.00000E+00
C     PROP  4.27315E-04
MO    PROP  1.46235E-05
MN    PROP  5.50350E-04
CU    PROP  2.90457E-05
SI    PROP  1.45148E-04
CO    PROP  3.77222E-06
ATOMS
MATERIAL  5 DENSITY 0.0
PU240 PROP  0.00000E+00
PU241 PROP  0.00000E+00
PU239 PROP  0.00000E+00
PU238 PROP  0.00000E+00
PU242 PROP  0.00000E+00
AM241 PROP  0.00000E+00
CR    PROP  1.18727E-03
NI    PROP  4.79539E-04
FE    PROP  4.27243E-03
AL    PROP  0.00000E+00
C     PROP  1.87078E-05
MO    PROP  8.23697E-06
MN    PROP  1.05699E-04
CU    PROP  1.71849E-05
SI    PROP  6.81747E-05
CO    PROP  0.00000E+00

END

***************************************************************************

BEGIN MATERIAL GEOMETRY

PART 1           ! six cylindrical boundaries
 ZROD 1         2*0.00  -38.17874 41.93313   76.35748
 ZROD 2         2*0.00  -92.08002 41.93313  184.16016
 ZROD 3         2*0.00  -92.08002 86.88175  184.16016
 ZROD 4         2*0.00  -92.08002 104.17047 184.16016
```

```
 ZROD 5         2*0.00  -121.9200 115.32402 243.84000
ZONES
/core/   M1   +1
/aref/   M2   +2 -1
/rref/   M3   +3 -2
/fref/   M4   +4 -3
/matrx/  M5   +5 -4
END

************************************************************************

BEGIN CONTROL DATA
STAGES -1  100  1000  STDV 0.0005
END

************************************************************************

BEGIN SOURCE GEOMETRY
ZONEMAT
 ALL / MATERIAL 1
END
```

A.5 VIM Input Listings

A sample VIM input is shown below. This input was used with continuous energy ENDF/B-V cross sections for all nuclides. The input for the calculations with continuous energy ENDF/B-VI cross sections is the same except that elements are replaced by their naturally occurring isotopes. All the cross sections correspond to 300 K. All the calculations were run with VIM Version 4.0 using 10,000 neutron histories per generation and 200 active generations, after skipping 40 generations. It would have been more computationally efficient to skip fewer generations, since the asymptotic fission source distribution was established by about the tenth generation.

```
VIM ENDF/B-V Input Listing, 4.1.

   397207447  rzr61024v5 - zpr6-10 -loading 24 - rz model - v5 xs
   200     3     0    40     0     0
 10000 10000     4     0     0     0
     1     1     0     0    50     0
    16     5     5    20     6 10000
 999999999.0 1.00000E-05 2.75000E+02 1.00000E+00 1.00000E-05 1.41910E+07
 9.50000E-01 0.00000E+00 1.00000E+00 0.00000E+00
     1     0     0     0     3     0     0     0     0     0     1     0
 10300 20300 50300 90300110300130300210300220300230300240300270300280300   08
290300340300380300560300                                                  08


    0     0     1
  CYL    1   0.00000   0.00000 -38.17900  76.35800  41.93313
  CYL    2   0.00000   0.00000 -92.08008 184.16016  41.93313
  CYL    3   0.00000   0.00000 -92.08008 184.16016  86.88175
  CYL    4   0.00000   0.00000 -92.08008 184.16016 104.17047
  CYL    5   0.00000   0.00000 -121.92   243.84    115.32402
  CYL    6   0.00000   0.00000    -200.0     400.0 150.00000
  END
  R01    6     +1
  R02    6     +2     -1
  R03    6     +3     -2
  R04    6     +4     -3
  R05    6     +5     -4
  R06    6     +6     -5
  END
     1 4.21812E+05     2 5.95514E+05     3 3.34987E+06     4 1.91100E+06
     5 4.33444E+06
     1   101   1             2   200   2             3   300   4
     4   400   5             5   500   3             6        -1
 10300 20300 50300 90300110300130300210300220300230300240300270300280300
290300340300380300560300
210300220300230300270300280300290300340300380300560300

210300220300230300270300280300290300340300380300

210300220300230300240300270300280300290300340300380300560300

210300220300230300270300280300290300340300380300560300

 5.03034E-05 1.70033E-06 1.06298E-03 1.69379E-09 1.15591E-07 2.98612E-06
 9.84196E-03 4.08528E-03 3.52607E-02 1.11659E-04 2.58213E-02 7.42790E-05
 8.05253E-04 1.01231E-04 2.79577E-04 3.71922E-06
 1.57277E-02 6.94658E-03 5.55223E-02 2.35876E-04 1.52118E-05 1.56081E-03
 2.98112E-05 9.45493E-04 3.73583E-06
 1.18727E-03 4.79539E-04 4.27243E-03 1.87078E-05 8.23697E-06 1.05699E-04
 1.71849E-05 6.81747E-05
 1.56286E-02 6.78410E-03 5.51964E-02 1.33185E-11 2.37106E-04 4.64023E-05
 1.42057E-03 5.04052E-05 8.63360E-04 3.77932E-06
 1.82758E-03 7.61435E-04 7.66532E-02 4.27315E-04 1.46235E-05 5.50350E-04
 2.90457E-05 1.45148E-04 3.77222E-06
  1.3000e+07  1.1000e+07  9.0000e+06  7.0000e+06  5.0000e+06  3.0000e+06
  1.0000e+06  8.0000e+05  6.0000e+05  4.0000e+05  2.0000e+05     90000.0
     70000.0     50000.0     30000.0     17000.0      9118.8      3000.0
       100.0        10.0  1.0000e-05
```

APPENDIX B: ADDITIONAL MODELS OF ZPR-6/10

The analyses presented in Appendix B were performed in 2002 for Revision 0 of this evaluation. They are retained here because B.1 shows the individual components of the transformation from the as-built model to the benchmark model and B.3 is another demonstration of the sensitivity of the calculated k_{eff} for this assembly to the specific version and processing of the nuclear data used for the calculation.

B.1 Decomposition of the As-Built-to-Benchmark Transformation

The individual effects of several simplifications that together comprise the transformation from the as-built model to the benchmark model of ZPR-6/10 were quantified. This was done to see the relative importance of each simplification and to confirm that the net effect does not involve partial cancellation of much larger components. The k_{eff} values for a sequence of four models are shown in Table B.1. These values were calculated using the VIM code with ENDF/B-V nuclear data. The model changes are cumulative and the models are progressively more simplified in successive rows of the table.

Table B.1 Progression of ZPR-6/10 Model Simplifications.

ID	Model Description	k-effective
A	XYZ plate-by-plate detail (As Built)	1.00086 ±0.00068
B	XYZ drawer-by-drawer detail (homogenized within each matrix position)	0.98498 ±0.00066
C	XYZ region-by-region detail, (homogenized within each region)	0.98614 ±0.00068
D	RZ region-by-region detail (Benchmark)	0.98625 ±0.00054

In Model B, all of the materials in a matrix location (i.e., plates, drawer, matrix tube, gaps, etc.) have been homogenized within that matrix location and within the axial (Z) ranges of the RZ benchmark model material regions. The k_{eff} difference $k_B - k_A = -0.0159 \pm 0.0009$ is the effect of unit cell homogenization. Although this is larger than the cell homogenization effect associated with benchmarks derived previously from ZPR assemblies, it is not unusual for ZPR assemblies in general.[a]

In Model C, all of the matrix locations within a benchmark model material region are homogenized. The k_{eff} difference $k_C - k_B = +0.0012 \pm 0.0009$ is the effect of smearing all the homogenized drawer types in a given region while maintaining the original XY outline of the region. For example, in the core region it represents the smearing of homogeneous normal core drawers, thermocouple drawers and PSR drawers. This effect is comparable in size to the statistical uncertainty.

In Model D, the XYZ regions become RZ regions that preserve cross sectional areas and volumes. The k_{eff} difference $k_D - k_C = +0.0001 \pm 0.0009$ is the effect of transforming the stepped outer boundaries of the XYZ model into the smooth cylindrical outer boundaries of the RZ model. It can only be claimed that this effect is unlikely to be larger that the statistical uncertainty.

The total transformation Δk in Section 3.5 is $k_D - k_A = -0.0147 \pm 0.0009$. The results above show that the only important component is the effect of homogenizing the plate units cells. The continuous energy Monte Carlo method, embodied in the VIM code, computes this effect with no approximations other than statistical sampling and use of ENDF/B-V neutron cross section data.

[a] A. L. Hess, R. G. Palmer and J. M. Stevenson, "A Postanalystical Study of Eight ZPR-3 Benchmark Criticals Using ENDF/B Data," in Argonne National Laboratory Report ANL-7710 (1971).

B.2 TWODANT Model of Benchmark Used for Sensitivity Calculations

Although none of the TWODANT calculations utilized a standard cross section set, the following sample input listing is provided because most of the sensitivity results in Section 2 are based on TWODANT calculations. These calculations used ENDF/B-V-based 20 group cross sections generated with the cross-section processing code MC^2-2.[a] This code, developed at Argonne National Laboratory, is available from the RSICC code center. Nuclide identifiers with a last letter "C" are appropriate in the core regions of the model, while identifiers ending with "R" are used in the reflector regions. This input corresponds to the RZ benchmark model specified in Section 3. It was used as a reference model that was modified in a variety of ways to obtain the sensitivity results presented in Section 2. All the calculations used the standard S_8 quadrature set, P_1 scattering order, a mesh spacing of 1.75 cm or less, and convergence criteria of 10^{-7}.

```
TWODANT Sample Input Listing

1
        zpr6-10_L24 benchmark P1 calculation
 igeom=7, ngroup=20, isn=08,
 niso=81, mt=05,     nzone=05,
 im=4,    it= 120,
 jm=3,    jt= 90,
 maxlcm=15000000, maxscm=10000000
  t
 xmesh=0.0 41.93313 86.88175 104.17047 115.32402,
 ymesh=0.0 38.17874 92.08002 121.92
 xints=45 40 20 15,
 yints=35 35 20,
 zones=1 3 4 5;
       2 3 4 5;
       5 5 5 5;
  t
 lib=isotxs
  t
 matls=
core P40HC  5.03037E-05, P41HC  1.70034E-06, P39HC  1.06299E-03,
     P38HC  1.69380E-09, P42HC  1.15592E-07, A41HC  2.98613E-06,
     CR-HC  9.84199E-03, NI-HC  4.08528E-03, FE-HC  3.52607E-02,
     AL-HC  1.11659E-04, C12HC  2.58213E-02, MO-HC  7.42792E-05,
     MN-HC  8.05254E-04, CU-HC  1.01231E-04, SI-HC  2.79577E-04,
     CO9HC  3.71924E-06;
aref CR-AR  1.57277E-02, NI-AR  6.94657E-03, FE-AR  5.55221E-02,
     C12AR  2.35948E-04, MO-AR  1.52120E-05, MN-AR  1.56081E-03,
     CU-AR  2.98115E-05, SI-AR  9.45490E-04, CO-AR  3.73582E-06;
rref CR-RR  1.56286E-02, NI-RR  6.78410E-03, FE-RR  5.51964E-02,
     AL-RR  1.33185E-11, C12RR  2.37106E-04, MO-RR  4.64023E-05,
     MN-RR  1.42057E-03, CU-RR  5.04052E-05, SI-RR  8.63360E-04,
     CO-RR  3.77932E-06;
fref CR-FR  1.82758E-03, NI-FR  7.61435E-04, FE-FR  7.66532E-02,
     C12FR  4.27315E-04, MO-FR  1.46235E-05, MN-FR  5.50350E-04,
     CU-FR  2.90457E-05, SI-FR  1.45148E-04, CO-FR  3.77222E-06;
matr CR-MR  1.18727E-03, NI-MR  4.79539E-04, FE-MR  4.27243E-03,
     C12MR  1.87078E-05, MO-MR  8.23697E-06, MN-MR  1.05699E-04,
     CU-MR  1.71849E-05, SI-MR  6.81747E-05
assign=CORE  core 1.0;
       AXREF aref 1.0;
       SSREF rref 1.0;
       FEREF fref 1.0;
       MATRX matr 1.0
  t
 ievt= 1,
 ith=  0,
 epsi=1.0E-07, epso=1.0E-07, iitl=1, iitm=100, oitm=100,
```

[a] H. Henryson II, B. J. Toppel, and C. G. Stenberg, "MC^2-2: A Code to Calculate Fast Neutron Spectra and Multigroup Cross Sections," Argonne National Laboratory Report ANL-8144 (1976).

```
ibl=  1, ibr=0, ibb=1, ibt=0,
isct= 1,

fluxp=0, xsectp=1, fissrp=0, sourcp=0, angp=0, balp=1,
raflux=0, rmflux=0,

geomp=1, influx=0, norm=0.0
 t
pted=1, zned=0, power=0.000001, ajed=0,
 t
```

The TWODANT calculation using this input yielded k_{eff} = 0.9875, which agrees well with both the experimental benchmark model k_{eff} and the VIM ENDF/B-V result for the benchmark model. The contrast with the much less accurate result from KENO-V with ENDF/B-V-based 238 group cross sections produced by SCALE[a] (k_{eff} = 1.0269 - see Section 4) points to the unusually high sensitivity of this benchmark to cross section processing. Since the benchmark has no geometric features that could challenge the capabilities of either KENO or TWODANT, the difference in multigroup cross section sets apparently is responsible for the k_{eff} difference. The MC^2-2 code was developed specifically for fast reactor applications, in which an accurate treatment of resolved and unresolved cross sections is important. It is shown in Appendix C that an unusually large fraction of the ZPR-6/10 neutron flux spectrum is in the resonance range. In addition, the MC^2-2 calculation of the ZPR-6/10 spectrum was done at the 2000 group level, whereas SCALE started at the 238 group level.

The most important issue, however, is likely to be processing errors due to resonance-like behavior in the ENDF/B high-energy "smooth" elastic-scattering cross sections of structural materials such as iron. This problem was identified and corrected in Argonne codes as a direct result of experience with ZPR-9/33 and ZPR-9/34 (HEU-MET-INTER-001).[b,c] A ZPR-6/10 benchmark model test calculation was run without self shielding this resonance-like data in the supporting MC^2-2 calculation and the resulting k_{eff} was 1.0161, an increase of nearly 3%.

B.3 Alternative Iron Cross Sections in MCNP Calculation of the Benchmark Model

All the isotopic cross sections specified for the MCNP 4C result with ENDF/B-V cross sections (see Section 4.0) were type 50c, which is the most current release of ENDF/B-V cross sections,[d] i.e., Version V.2. This calculation was repeated with the only input difference being specification of type 55c (a special LANL evaluation) for iron. The computed k_{eff} changed from 0.9945 ±0.0005 to 0.9699 ±0.0005, a decrease of 0.0246 ±0.0007. The sensitivity is strong and the results are more accurate with ENDF/B-V iron cross sections. This is similar to the results of the same test made for the Uranium/Iron Benchmark (see Appendix B of HEU-MET-INTER-001).

[a] Although the 238 group library has ENDF/B-VI-based data for five nuclides, none of these nuclides is present in the ZPR-6/10 benchmark.
[b] R. D. McKnight, R. N. Hwang, C. G. Stenberg and R. N. Blomquist, "Validation Studies of the ENDF/MC^2-2/SDX Cell Homogenization Path," Proceedings of the Topical Meeting on Advances in Reactor Physics and Core Thermal Hydraulics, Kiamesha Lake, NY, September 22-24, 1982, pp. 406-423 (1982).
[c] R. N Hwang, B. J Toppel and H. Henryson II, "Improved Algorithms for the Calculation of Resolved Resonance Cross Sections with Applications to the Structural Doppler Effect in Fast Reactors, Argonne National Laboratory Report, ANL-80-104, October 1980.
[d] Private communication, R. D. Mosteller, April 28, 1998.

APPENDIX C: SPECTRUM AND NEUTRON BALANCE FROM VIM

Figure C.1 shows the core-average spectrum in ZPR-6/10 along with that in two other benchmark assemblies, ZPR-3/41 (IEU-MET-FAST-012) and Jezebel (PU-MET-FAST-001). All of these spectra were computed with the VIM code and continuous-energy ENDF/B-V data. Each energy bin width for the flux edits corresponds to a lethargy change of 0.25 ($E_{g-1}/E_g = 1.284$) from ~14 MeV to ~1 keV, except for one adjustment to get a boundary exactly at 100 keV. Below there the bins are broader. The spectra are normalized so that the integral of the flux over all energies is unity.

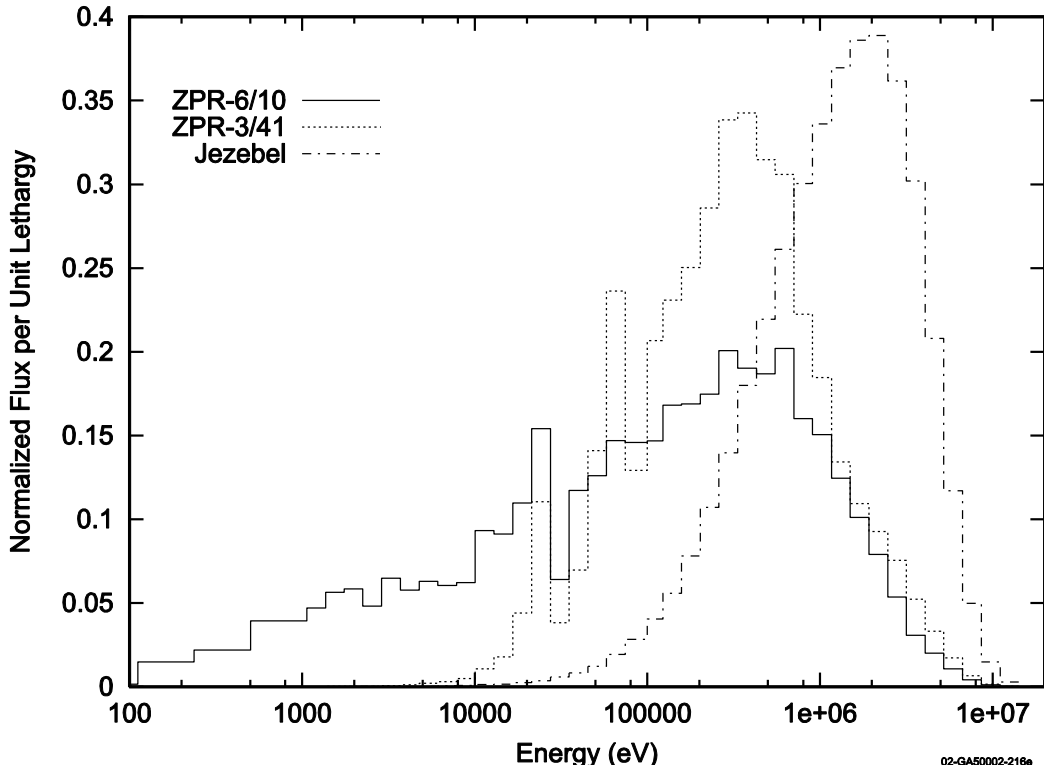

Figure C.1. Core-Average Neutron Spectra in ZPR-6/10, ZPR-3/41 and Jezebel.

The spectrum comparison is revealing. Jezebel was a sphere of essentially pure plutonium. ZPR-3/41 was an early simulation of a uranium-fueled LMFBR, with aluminum as a surrogate for the sodium coolant. It is no surprise that the spectrum in Jezebel is much harder and narrower than that in the ZPR cores, since Jezebel contained no moderating materials. The interesting observation is that, although the two ZPR spectra peak at about the same energy, the ZPR-6/10 spectrum is much flatter, with a tail extending down to 100 eV. This is attributable to the large amount of graphite moderator in the ZPR-6/10 core.

A consequence is that resonance cross sections have an unusually strong influence on k_{eff}. The high importance of the resonance energy range was a deliberate feature of ZPR-6/10; a major portion of the ZPR-6/10 experimental program was a study of the influence of the resonance range on the ^{238}U capture rate, both in the reference core and in a core zone containing ^{238}U. The most abundant constituents of stainless steel - Cr, Fe and Ni - have large resonances between 4 keV and 70 keV, a range where the ZPR-6/10 flux level is unusually high. The "iron window", caused by a large iron scattering resonance near 28 keV, is evident in the ZPR-6/10 spectrum. Mn has strong resonances between 200 eV and 20 keV, and the extraordinary flux level there explains why the ZPR-6/10 k_{eff} is so sensitive to the uncertainty in the concentration of this stainless steel constituent (see Section 2). Probably the most important impact on k_{eff} of the strong low-energy flux comes from the ^{239}Pu resonances. The flux level is significant at the upper end of ^{239}Pu resolved resonance range, 1 eV to 301 eV, and it is very important in the unresolved-resonance range, 301eV to 25 keV. The latter fact explains why the calculated k_{eff} changed almost 1% when the improved unresolved resonance range treatment, embodied in MCNP 4C, was used in place of the treatment in MCNP 4B (see Section 4).

The core spectra from the VIM ENDF/B-V as-built and RZ calculations of ZPR-6/10 should be very similar. These spectra are compared in Figure C.2 and it can be seen that they are quite similar. The only noticeable difference is that the RZ model flux is a little higher above 8 keV and is a little lower below there, particularly below 300 eV. The very fine group structure (199 groups) shows the large flux swings caused by the resonance cross sections.

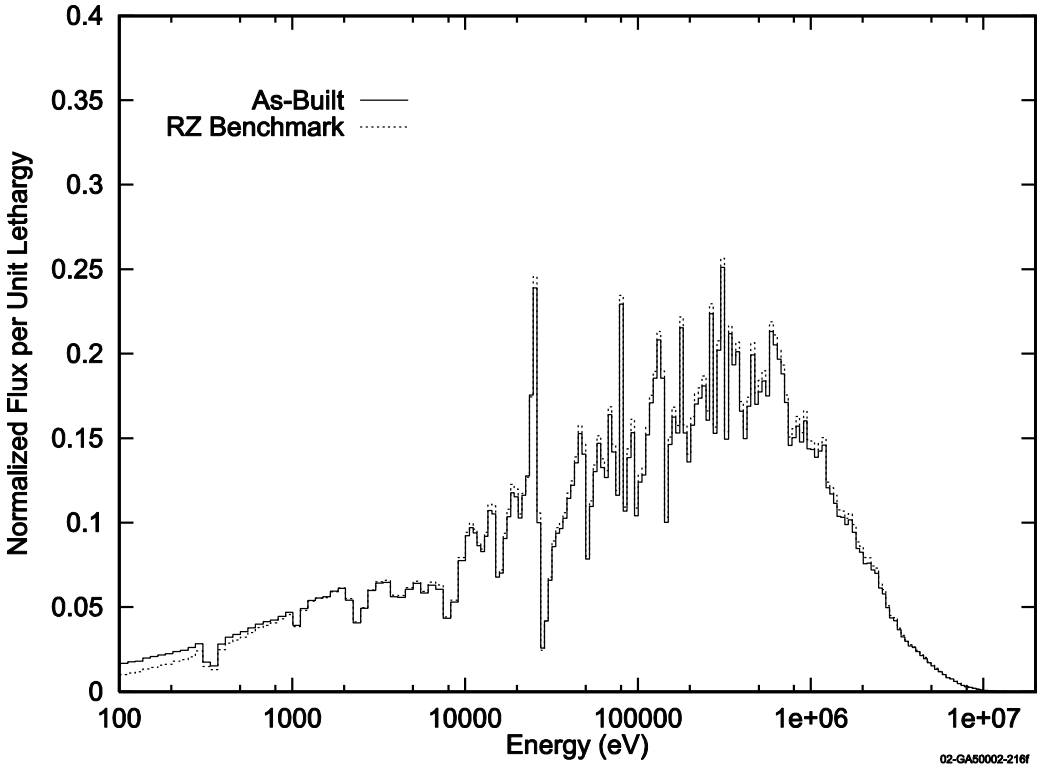

Figure C.2. Comparison of Core Spectra From ZPR-6/10 As-Built and RZ Benchmark Models.

The track-length-estimator neutron balance edit indicates that ZPR-6/10 falls into the intermediate-energy spectrum category (INTER) of ICSBEP benchmarks. The flux above 100 keV produced 35% of the fissions, essentially none was produced by the flux below 0.625 eV, and 65% was produced by the flux between these energies.

The following global neutron balance for ZPR-6/10 was obtained from the calculation with the VIM code using the as-built model. The track-length estimator provided the total production and losses for the entire model as follows:

Fission Production	1.0011 ± 0.0007
(n,2n) Production	0.0001 ± 2%
Absorption	0.9396 ± 0.0006
Leakage	0.0604 ± 0.0006
k_{eff}	1.0012 ± 0.0008

The final result with ENDF/B-V data given in Section 3.5, $k_{eff} = 1.00086 \pm 0.0007$, is slightly different from (though consistent with) the track-length estimator because it is the combination of the analog and track-length estimators (accounting for the correlation between them). Two partial sums are unity: absorption plus leakage, and fission production/k_{eff} plus (n,2n) production. The ratio of leakage to fission production for this assembly is ~6.0%.

The detailed, track-length-estimator neutron balance from the ZPR-6 Assembly 10 as-built model is summarized in Table C.1. It shows, for each nuclide and region, the neutron production by fission and (n,2n) reactions, and the losses by neutron absorption and leakage. The reaction rates are integrated over the total volume of the region and the leakage is the net leakage over the surface of the region (i.e., the combination of the positive leakage out of the region and negative leakage of neutrons returning to the region). Note the total leakage quoted above is the leakage for the full model. As shown in Table C.1, the fission rate is dominated by ^{239}Pu. ^{239}Pu capture accounts for about half the capture rate in the core region, and nearly all the remainder is accounted for by the four main constituents of stainless steel (Cr, Ni, Fe and Mn). Leakage from the core is ~39%, most of which is absorbed in the stainless steel reflector regions.

Table C.1. As-Built Model Neutron Balance by Nuclide and Region for ZPR-6/10.[a]

Core Region					
Nuclide	**Fission Production**	**Fission**	**Capture**	**Absorption**	**n,2n Production**
^{240}Pu	9.5330E-03	3.1361E-03	9.9996E-03	1.3136E-02	1.5894E-06
^{241}Pu	2.9484E-03	9.9233E-04	2.4256E-04	1.2349E-03	7.7205E-07
^{239}Pu	9.8804E-01	3.3661E-01	1.2990E-01	4.6650E-01	7.4422E-05
^{238}Pu	6.2310E-07	2.0754E-07	2.8444E-07	4.9198E-07	1.0317E-10
^{242}Pu	1.3405E-05	4.3456E-06	2.9787E-05	3.4132E-05	1.2960E-08
^{241}Am	5.6298E-04	1.6572E-04	1.4672E-03	1.6330E-03	7.7980E-08
Cr			3.0691E-02	3.0691E-02	2.0067E-05
Ni			1.7196E-02	1.7196E-02	1.0524E-06
Fe			5.5196E-02	5.5196E-02	1.5154E-05
Al			4.7467E-05	4.7467E-05	8.5849E-10
C			3.0207E-04	3.0207E-04	0.0000E+00
Mo			4.2009E-03	4.2009E-03	2.3531E-06
Mn			1.7466E-02	1.7466E-02	1.5317E-06
Cu			1.6834E-03	1.6834E-03	1.3938E-07
Si			1.1022E-04	1.1022E-04	8.0689E-08
Co			5.2544E-04	5.2544E-04	5.0653E-09
Region Sum	1.001100	0.340910	0.269060	0.609960	0.000117
Leakage	0.390030				
Axial Stainless Steel Reflector					
Cr			1.6994E-02	1.6994E-02	1.0535E-06
Ni			9.3127E-03	9.3127E-03	6.4966E-08
Fe			3.5075E-02	3.5075E-02	9.5181E-07
C			2.2048E-07	2.2048E-07	0.0000E+00
Mo			4.4453E-04	4.4453E-04	1.6329E-08
Mn			1.1664E-02	1.1664E-02	1.0579E-07
Cu			1.5614E-04	1.5614E-04	1.4285E-09
Si			8.3593E-05	8.3593E-05	9.0109E-09
Co			2.5338E-04	2.5338E-04	2.1285E-10
Region Sum			0.073984	0.073984	0.000002
Leakage	-0.073981				

Table C.1. (cont'd.) As-Built Model Neutron Balance by Nuclide and Region for ZPR-6/10.[(a)]

Nuclide	Fission Production	Fission	Capture	Absorption	n,2n Production
Radial Stainless Steel Reflector					
Cr			5.5321E-02	5.5321E-02	2.7585E-06
Ni			2.9759E-02	2.9759E-02	1.6069E-07
Fe			1.1534E-01	1.1534E-01	1.8974E-06
C			6.6612E-07	6.6612E-07	0.0000E+00
Mo			5.4674E-03	5.4674E-03	1.6824E-07
Mn			3.4499E-02	3.4499E-02	2.5727E-07
Cu			1.0129E-03	1.0129E-03	8.4257E-09
Si			2.3577E-04	2.3577E-04	2.2168E-08
Co			8.4997E-04	8.4997E-04	6.2596E-10
Region Sum			0.242490	0.242490	5.2733E-06
Leakage	-0.242480				
Radial Iron Reflector					
Cr			4.5699E-04	4.5699E-04	3.1917E-10
Ni			2.4399E-04	2.4399E-04	5.5806E-11
Fe			1.0858E-02	1.0858E-02	9.4369E-09
C			6.1686E-08	6.1686E-08	0.0000E+00
Mo			9.0103E-05	9.0103E-05	3.9568E-11
Mn			1.0223E-03	1.0223E-03	3.5164E-10
Cu			2.9726E-05	2.9726E-05	1.2713E-11
Si			2.7395E-06	2.7395E-06	7.4718E-12
Co			5.1469E-05	5.1469E-05	2.5231E-12
Region Sum			0.012755	0.012755	1.0226E-08
Leakage	-0.012755				

Table C.1. (cont'd.) As-Built Model Neutron Balance by Nuclide and Region for ZPR-6/10.[(a)]

Empty Matrix					
Nuclide	**Fission Production**	**Fission**	**Capture**	**Absorption**	**n,2n Production**
Cr			1.0817E-04	1.0817E-04	
Ni			5.6506E-05	5.6506E-05	
Fe			2.1272E-04	2.1272E-04	
C			8.0961E-10	8.0961E-10	
Mo			1.9083E-05	1.9083E-05	
Mn			5.6204E-05	5.6204E-05	
Cu			7.0373E-06	7.0373E-06	
Si			5.3914E-07	5.3914E-07	
Region Sum			0.000460	0.000460	
Leakage	-0.000460				
Totals for As-Built Model					
Sum	1.001100	0.340910	0.598740	0.939650	0.000125
Total Leakage	0.060352				
k_{eff}	1.001219				

(a) The normalization is such that (Absorption + Leakage) = (Fission Production) / k_{eff} + (n,2n) = 1.0.

The neutron balance from the VIM ENDF/B-V calculation of the RZ benchmark model should be very similar to the as-built model neutron balance just presented. To confirm this, the RZ results are displayed here in the same format. The track-length estimator provided the total production and losses for the entire model as follows:

Fission Production	0.9866 ±0.0010
(n,2n) Production	0.0001 ± 2%
Absorption	0.9385 ± 0.0008
Leakage	0.0615 ± 0.0008
k_{eff}	0.9867 ± 0.0010

The main change from the corresponding as-built results is a ~1.5% decrease in fission production compared to total losses. This is consistent with the fact, established in Appendix B, that the dominant component of the transformation Δk is removal of the plate cell heterogeneity. The uniform distribution of the fuel in the homogeneous cell, compared to the narrow column of fuel in the plate cell, decreases the fission production.

The RZ benchmark model detailed neutron balance is displayed in Table C.2. Compared to the core region balance in the as-built calculation, both the fission and capture rates in the fuel are lower, while the capture rate in the steel is higher by enough to make the total core absorption slightly higher. This is consistent with the flux peaking at the fuel column of the plate unit cell. Most of the neutron balance changes from the as-built case are quite small.

Table C.2. RZ Benchmark Model Neutron Balance by Nuclide and Region for ZPR-6/10.[(a)]

Core Region					
Nuclide	**Fission Production**	**Fission**	**Capture**	**Absorption**	**n,2n Production**
^{240}Pu	7.6117E-03	2.5357E-03	9.2297E-03	1.1765E-02	7.6836E-07
^{241}Pu	2.4386E-03	8.2184E-04	1.9448E-04	1.0163E-03	3.7661E-07
^{239}Pu	9.7616E-01	3.3428E-01	1.5306E-01	4.8734E-01	3.6495E-05
^{238}Pu	8.7206E-07	2.9252E-07	3.6063E-07	6.5315E-07	7.9308E-11
^{242}Pu	1.2728E-05	4.1752E-06	1.7125E-05	2.1300E-05	7.7054E-09
^{241}Am	4.1410E-04	1.2329E-04	1.2190E-03	1.3423E-03	3.7396E-08
Cr			2.7998E-02	2.7998E-02	1.9966E-05
Ni			1.5661E-02	1.5661E-02	1.0429E-06
Fe			4.7304E-02	4.7304E-02	1.5414E-05
Al			4.2523E-05	4.2523E-05	7.4128E-10
C			3.3378E-04	3.3378E-04	0.0000E+00
Mo			2.9692E-03	2.9692E-03	2.3181E-06
Mn			1.5020E-02	1.5020E-02	1.4968E-06
Cu			1.5780E-03	1.5780E-03	1.3888E-07
Si			1.0800E-04	1.0800E-04	8.1796E-08
Co			3.2608E-04	3.2608E-04	6.0481E-09
Region Sum	0.986640	0.337770	0.275060	0.612830	0.000078
Leakage	0.387170				
Axial Stainless Steel Reflector					
Cr			1.6545E-02	1.6545E-02	1.2580E-06
Ni			9.0353E-03	9.0353E-03	6.1712E-08
Fe			3.3724E-02	3.3724E-02	6.9591E-07
C			2.3905E-07	2.3905E-07	0.0000E+00
Mo			4.5219E-04	4.5219E-04	1.9262E-08
Mn			1.1275E-02	1.1275E-02	1.1141E-07
Cu			1.6533E-04	1.6533E-04	1.5526E-09
Si			8.6560E-05	8.6560E-05	1.1459E-08
Co			2.5984E-04	2.5984E-04	2.2204E-10
Region Sum			0.071544	0.071544	0.000002
Leakage	-0.071541				

Table C.2. (cont'd.) RZ Benchmark Model Neutron Balance by Nuclide and Region for ZPR-6/10.[(a)]

Nuclide	Fission Production	Fission	Capture	Absorption	n,2n Production
Radial Stainless Steel Reflector					
Cr			5.4997E-02	5.4997E-02	2.7901E-06
Ni			2.9625E-02	2.9625E-02	1.6805E-07
Fe			1.1361E-01	1.1361E-01	2.8132E-06
C			6.7661E-07	6.7661E-07	0.0000E+00
Mo			4.5764E-03	4.5764E-03	1.2118E-07
Mn			3.5229E-02	3.5229E-02	2.3361E-07
Cu			9.1184E-04	9.1184E-04	6.3316E-09
Si			2.5135E-04	2.5135E-04	2.1495E-08
Co			8.8753E-04	8.8753E-04	5.6112E-10
Region Sum			0.240090	0.240090	0.000006
Leakage	-0.240090				
Radial Iron Reflector					
Cr			4.9244E-04	4.9244E-04	7.3915E-10
Ni			2.6014E-04	2.6014E-04	7.4200E-12
Fe			1.1490E-02	1.1490E-02	0.0000E+00
C			6.7617E-08	6.7617E-08	0.0000E+00
Mo			9.9084E-05	9.9084E-05	7.1315E-11
Mn			1.0893E-03	1.0893E-03	0.0000E+00
Cu			3.2052E-05	3.2052E-05	0.0000E+00
Si			2.9302E-06	2.9302E-06	1.2146E-12
Co			5.7146E-05	5.7146E-05	0.0000E+00
Region Sum			0.013523	0.013523	8.1910E-10
Leakage	-0.013523				

Table C.2. (cont'd.) RZ Benchmark Model Neutron Balance by Nuclide and Region for ZPR-6/10.[(a)]

Empty Matrix					
Nuclide	**Fission Production**	**Fission**	**Capture**	**Absorption**	**n,2n Production**
Cr			1.1578E-04	1.1578E-04	
Ni			6.1299E-05	6.1299E-05	
Fe			2.1909E-04	2.1909E-04	
C			9.0219E-10	9.0219E-10	
Mo			1.8517E-05	1.8517E-05	
Mn			6.1693E-05	6.1693E-05	
Cu			7.1628E-06	7.1628E-06	
Si			5.7275E-07	5.7275E-07	
Region Sum			0.000484	0.000484	
Leakage	-0.000484				
Totals for RZ Benchmark Model					
Sum	0.986640	0.337770	0.600700	0.938470	0.000086
Total Leakage	0.061532				
k_{eff}	0.986725				

(a) The normalization is such that (Absorption + Leakage) = (Fission Production) / k_{eff} + (n,2n) = 1.0.